Estimation of Relative Permittivity and Thickness for Dielectric Materials Using an Open-Ended Waveguide Sensor

Bahareh Nikparvar

Department of Physics and Technology

University of Bergen

A thesis submitted for the degree of

Master in Measurement Technology and Instrumentation

September 10, 2016

b

Abstract

The main goal of this thesis has been to conduct a feasibility study on an open-ended waveguide sensor as a tool for estimating the relative permittivity and thickness of dielectric layers in the thickness range 0.5–5 cm. To achieve this purpose, a reflection coefficient measurement technique was implemented. This non-destructive technique can be a potential method for characterization and configuration of gas hydrate deposition in oil and gas production. Microwaves which are emitted from a network analyzer, propagate through a waveguide sensor, interact with the dielectric material in front of the waveguide, and reflect back. Material and physical properties of the dielectric Material Under Test (MUT), particularly its relative permittivity and thickness, affect the reflected signal. These two parameters can therefore be estimated from the measured reflection coefficient.

Calibration of the measurement results was performed using a COMSOL simulation model of the experimental setup. By doing so, the measured reflection coefficients were transformed to the calibrated (transformed) reflection coefficients through a bilinear transformation formula. The COMSOL simulation model was also used to generate permittivity and thickness lookup matrices. The transformed reflection coefficient at different frequencies was mapped to the matrices to estimate the relative permittivity and thickness of the dielectric MUT.

To verify the relative permittivity estimation method, the reflection coefficient for three MUTs, ethanol/water mixtures with 0.36, 0.54, and 0.76 molar fractions, was measured in the frequency range 0.5–10 GHz and for a thickness of 3 cm. The measured reflection coefficients were converted to the transformed reflection coefficients. Then, using the permittivity lookup matrix and the transformed reflection coefficients, the relative permittivity was estimated for each fluid in the frequency range 4–10 GHz. In the range 4–6 GHz, the estimation method provided satisfactory results with an estimation error of 20.21%, 11.37%,

and 3.80% for the three fluids, respectively. However, in the range 6–10 GHz, the results were not acceptable mainly due to interference between the dominant propagation mode and higher order modes in the waveguide.

Additionally, the reflection coefficient was measured for the above mentioned mixtures in the thickness range 0.5–3 cm. The thickness was estimated using the thickness lookup matrix. For thin layers up to 1 cm, there was a good agreement between the estimated and actual thickness values with an estimation error around 20%; whereas, for layers thicker than 1 cm, the error was more than 50%. It was found that the maximum detectable thickness was inversely proportional to the loss factor of the MUT. In case of MUTs with high loss factors, the estimation procedure gave acceptable results only for layers up to 1 cm. By contrast, for low-loss fluids such as diesel, it was found that the method provided satisfactory results for the thickness values up to 5 cm. The mean value of the thickness estimation error for diesel was found to be 6.37% in the range 0.5–5 cm.

Acknowledgements

I would first like to thank my supervisor senior scientist Kjetil Folgerø at Christian Michelsen Research. The door to his office was always open whenever I ran into a trouble spot or had a question about my research or writing. He consistently allowed this paper to be my own work, but steered me in the right direction whenever he thought I needed it.

I would like to express my sincere gratitude to my supervisor professor Bjørn Tore Hjertaker at University of Bergen for his encouragement, guidance and support during my master project. He has always been there for me to help with the project issues.

This work would not have been possible without the support from Christian Michelsen Research. I will not forget all the help I have received, especially during the experimental work, from scientist Kjetil Haukalid.

I thank technical product manager Bertil Nistad at COMSOL for his advices in the use of software COMSOL.

I would like to acknowledge also my friends at University of Bergen.

I cannot finish this page without a great deal of gratitude to my dear family for bringing me up, nurturing me along the way, and supporting me through the years. Last, but never least, my beloved husband Majid, for that optimism that gave me a glimmer of hope when all was dark. This work would be impossible without his support and care.

Contents

List of Figures

List of Tables

Abbreviations and Symbols

Acronyms

EM	Electromagnetic Wave
FEM	Finite Element Method
KHI	Kinetic Hydrate Inhibitors
MUT	Material Under Test
PML	Perfectly Matched Layer
RF	Radio Frequency
TE	Transverse Electric
TEM	Transverse Electric and Magnetic
TM	Transverse Magnetic

Electromagnetic Symbols

α	Distribution factor/Attenuation constant
β	Phase constant
$\mathbf{B}$	Magnetic field
$\mathbf{D}$	Electric displacement
$\mathbf{E}$	Electric field
$\mathbf{H}$	auxiliary field
$\mathbf{P}$	Polarization
$\hat{\mathbf{n}}$	Normal unit vector of the surface
χ_e	Electric susceptibility
χ_M	Magnetic susceptibility
γ	Wave propagation constant
λ	Wavelength of the electromagnetic wave

LIST OF TABLES

λ_{mn}	Waveguide cutoff wavelength
μ^*	Complex permeability
μ_0	Permeability of free space
ω	Angular frequency
ρ	Total charge density
ρ_b	Volume bound charge density
σ	Conductivity
σ_b	Surface bound charge density
τ	Relaxation time
$\varepsilon_r^{''}$	Loss factor
$\varepsilon_r^{'}$	Relative dielectric constant
ε^*	Complex permittivity
ε_r^*	Complex relative permittivity
ε_0	Permittivity of free space
ε_∞	Infinite permittivity
ε_s	Static permittivity
A, B, $and\, C$	Bilinear transformation coefficients
c	Velocity of light
E_{ij} $i, j = 1, 2$	Scattering parameters of the error network
f	Frequency
f_d	Dispersion frequency
f_{mn}	Waveguide cutoff frequency
k	Wave number
m/n	Number of half-wavelength variations of field in the larger/shorter dimension of the waveguide opening
S_{11}^M	Measured reflection coefficient
S_{11}^R	Reference (transformed) reflection coefficient
S_{11}, S_{22}	Reflection coefficient
S_{12}, S_{21}	Transmission coefficient
$tan\delta$	Dissipation factor

v	Velocity of wave propagation

Material and Test Object Symbols

a	larger dimension of the waveguide opening (width of the waveguide)
b	Shorter dimension of the waveguide opening (height of the waveguide)
d	Thickness of MUT layer

Statistical Symbols

$\bar{x}$	mean value
s	Standard deviation
u	standard uncertainty of a new measurement
u_{avg}	standard uncertainty of the mean value

Chapter 1

Introduction

Relative permittivity estimation is a non-destructive method for dielectric material characterization, particularly in non-accessible environments. Additionally, layer thickness estimation can provide some information about the structure of the environment. The relative permittivity and thickness estimation is beneficial in many different industrial fields such as monitoring gas hydrate formation in pipelines. In this project, microwaves were guided in a specific path using an open-ended waveguide sensor to interact with a layer of dielectric Material Under Test (MUT), and reflected back while carrying information about the characteristics of the layer. A reflection coefficient measurement technique was utilized to estimate the relative permittivity and thickness. The feasibility of this approach was verified by comparing the actual and estimated values of the relative permittivity and thickness.

1.1 Aim of Project and Methodology of Work

The main goal of this master project was to conduct a feasibility study on an open-ended waveguide sensor as a tool for estimating the relative permittivity and thickness of dielectric layers in range of a few centimeters. An open-ended waveguide sensor radiates a large fraction of energy into the layer, which is installed in front of the waveguide. Thus, by analyzing the received signal reflected back from the end-point of the layer (i.e. reflection coefficient), the relative permittivity and thickness of the layer can be estimated. Figure 1.1 shows a schematic drawing of an open-ended waveguide sensor used to measure the reflection coefficient.

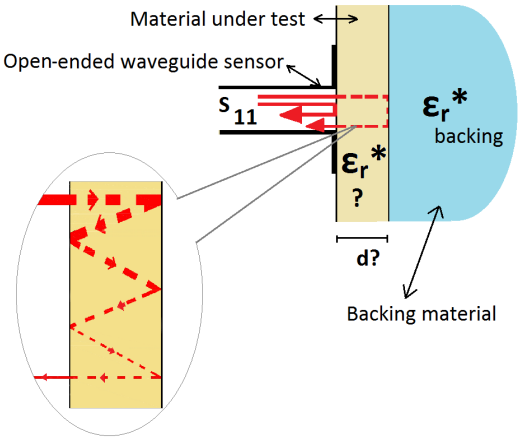

Figure 1.1: A schematic drawing of using an open-ended waveguide sensor for estimating the relative permittivity (ε_r^*) and thickness (d) of a dielectric MUT. The reflection coefficient, S_{11}, includes the main reflection from the interface between the waveguide sensor and the MUT layer (solid red line), and the secondary reflections through the layer (dashed red line).

The methodology of the work was composed of:

1. Developing a simulation model using COMSOL multiphysics: the model of the experimental setup provides two functions; A) calibrating the waveguide sensor, B) generating a permittivity lookup matrix and a thickness lookup matrix. The former gives the simulated reflection coefficient as a function of frequency and relative permittivity for a specific thickness. The latter provides the simulated reflection coefficient as a function of frequency and thickness for a specific relative permittivity.

2. Measuring the reflection coefficient for specific fluids to calibrate the sensor: a frequency dependent relationship (via a bilinear transformation) between a set of the measured data and the simulated data provided a tool to calibrate the rest of the measured data. By doing so, the measured reflection coefficients were converted to the "transformed reflection coefficients".

3. Theoretical studies to develop a method for estimating the relative permittivity and layer thickness from the transformed reflection coefficients: by comparing the transformed reflection coefficients of a layer (with a specific thickness) with the elements of the permittivity lookup matrix, the relative permittivity of the layer at different frequencies was estimated. In case of estimating the thickness, the transformed reflection coefficients for a specific

relative permittivity were compared with the elements of the thickness lookup matrix. Figure 1.2 shows schematically the principle of estimating the relative permittivity and thickness of the MUT using the transformed reflection coefficients.

4. Verification of the above mentioned relative permittivity and thickness estimation method.

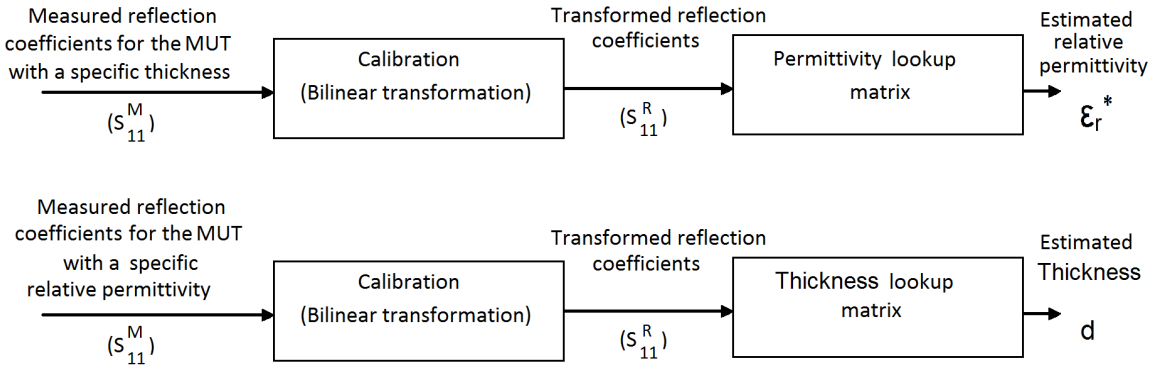

Figure 1.2: A block diagram showing the principle of estimating the relative permittivity and thickness from the transformed reflection coefficients.

1.2 Background and Motivation

Natural gas hydrate is an ice-like material which may be formed in oil and gas production, transportation, and processing facilities. This composite consists of water molecules interconnected through hydrogen bonds which create an open structural lattice that has the ability to encage smaller hydrocarbons such as methane or ethane (Figure 1.3). Gas hydrates are formed under low temperature and high pressure conditions that can occur in an oil and gas production process.

Since hydrates of natural gas can plug and damage equipment of gas transport systems, preventative methods have been studied worldwide for many years [2]. Current methods for avoiding gas hydrate problems are generally based on one or a combination of the following three techniques: (1) injection of thermodynamic inhibitors (e.g. methanol, ethylene glycol) to prevent the hydrate formation, (2) use of kinetic hydrate inhibitors (KHIs) to sufficiently delay hydrate growth, and

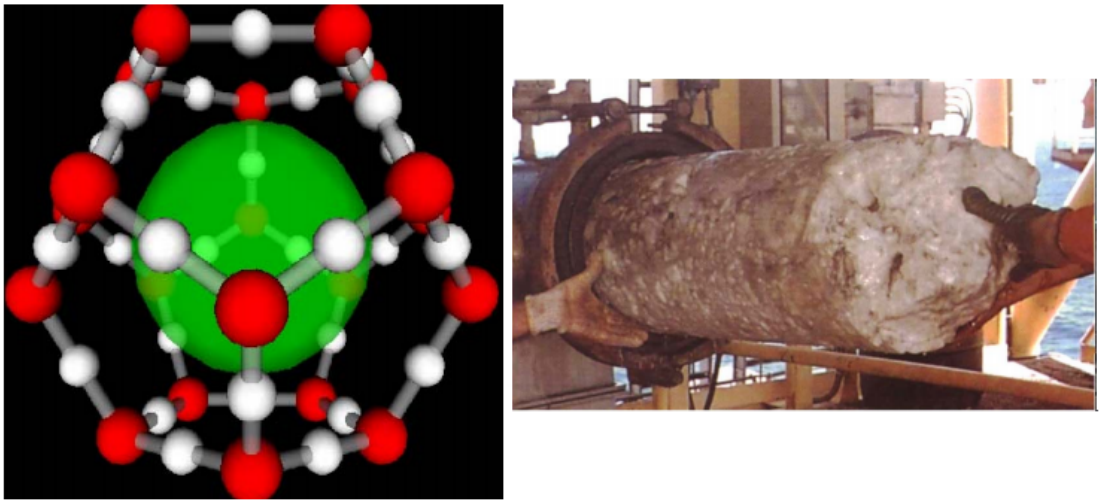

Figure 1.3: (a) Hydrates are crystalline solids wherein guest (generally gas) molecules are trapped in cages formed from hydrogen bonded water molecules (host). (b) This deposit can be formed in an oil and gas production process [1].

(3) maintaining pipeline operating conditions outside the hydrate stability zone by insulation, active heating, or by controlling pressure. However, for many production operations, these techniques may not be economical, environmental, nor logistically practical [3].

One way of monitoring the gas hydrate formation is to study the dielectric properties of the bulk, and particularly the relative permittivity. The formation of gas hydrates in emulsions gives rise to a change in the bulk relative permittivity. Dielectric spectroscopy is therefore a potential technique for detection of gas hydrates in emulsified systems and hydrate deposits on pipe walls [4]. Layer thickness is another property which can provide information about different stages of the hydrate formation. This technique can also be useful to characterize other deposits and layers for example wax, ice, snow, soil, mud, etc. In this thesis, a reflection coefficient measurement technique was used in order to estimate the relative permittivity and thickness of dielectric materials.

1.3 Thesis Organization

Chapter 2 contains relevant theories including polarization and permittivity, electromagnetic wave propagation in waveguides, and scattering parameters. Following, the existing permittivity measurement techniques are presented. The main contribution of this master project was to propose a non-destructive method for estimating the relative permittivity and thickness of dielectric layers, which is presented at the end of Chapter 2. Chapter 3 concerns the COMSOL simulation model and its two functions in this project i.e. calibrating the experimental setup and generating the lookup matrices for permittivity and thickness. A description of the experimental setup and experimental results are presented in Chapter 4. In Chapter 5, the estimated relative permittivity and thickness values are compared with the actual values and the accuracy of the proposed estimation procedure is discussed. Finally in Chapter 6, the main achievements of this work are summarized and some further research works are suggested.

This page is intentionally left blank

Chapter 2

Measurement of Permittivity

In this chapter, the relevant theories related to this master project are presented (Section 2.1) followed by a literature survey of permittivity measurement methods (Section 2.2). Finally the methodology of the permittivity and thickness estimation as the main contribution of this project is explained (Section 2.3).

2.1 Theory

2.1.1 Polarization

When a piece of a dielectric material consisting of neutral atoms (or non-polar molecules) is placed in an electric field $\mathbf{E}$, the field will induce in each a tiny dipole moment, pointing in the same direction as the field. If the material is made up of polar molecules, each permanent dipole will experience a torque, tending to align it along the field direction. These two mechanisms produce the same basic result: a lot of small dipoles pointing along the direction of the field and the material becomes polarized. A convenient measure of this effect is $\mathbf{P} \equiv$ *dipole moment per unit volume*, which is called polarization [5].

Polarization causes a certain distribution of surface and volume bound charge densities (σ_b and ρ_b, respectively) formed on the surface and within the dielectric:

$$\begin{aligned} \sigma_b &\equiv \mathbf{P} \cdot \hat{\mathbf{n}} \\ \rho_b &\equiv -\nabla \cdot \mathbf{P} \end{aligned} \tag{2.1}$$

where $\hat{\mathbf{n}}$ is the normal unit vector of the surface. Within the dielectric, the total charge density can be written as:

$$\rho = \rho_b + \rho_f \tag{2.2}$$

where ρ_f is the volume free charge density. The free charge might consist of electrons on a conductor or ions embedded in the dielectric material or any charge that is not result of the polarization. From Gauss's law:

$$\begin{aligned} \varepsilon_0 \nabla \cdot \mathbf{E} = \rho = \rho_b + \rho_f = -\nabla \cdot \mathbf{P} + \rho_f \\ \nabla \cdot (\varepsilon_0 \mathbf{E} + \mathbf{P}) = \rho_f \end{aligned} \tag{2.3}$$

where ε_0 is the permittivity of free space ($8.854 \times 10^{-12}\, F/m$). In Eq. 2.3 the expression in parentheses is known as the electric displacement ($\mathbf{D}$),

$$\begin{aligned} \mathbf{D} \equiv \varepsilon_0 \mathbf{E} + \mathbf{P} \\ \nabla \cdot \mathbf{D} = \rho_f. \end{aligned} \tag{2.4}$$

2.1.2 Susceptibility, Permittivity, and Dielectric Constant

For many substances, the polarization is proportional to the electric field, provided $\mathbf{E}$ is not too strong:

$$\mathbf{P} = \varepsilon_0 \chi_e \mathbf{E} \tag{2.5}$$

where the constant of proportionality, χ_e, is called electric susceptibility of the medium. This value depends on the microscopic structure of the substance in question (and also external conditions such as temperature). Materials that obey Eq. 2.5 are called linear dielectrics. For a linear media:

$$\begin{aligned} \mathbf{D} = \varepsilon_0 \mathbf{E} + \mathbf{P} = \varepsilon_0 \mathbf{E} + \varepsilon_0 \chi_e \mathbf{E} = \varepsilon_0 (1 + \chi_e) \mathbf{E} \\ \mathbf{D} = \varepsilon \mathbf{E} \end{aligned} \tag{2.6}$$

where

$$\varepsilon = \varepsilon_0 \cdot (1 + \chi_e). \tag{2.7}$$

ε is the permittivity of the material which is a complex value that depends on frequency and temperature. Therefore, it is typically referred to as ε^*.

Eq. 2.7 can be restated as:

$$\varepsilon^* = \varepsilon_0 \cdot \varepsilon_r^* = \varepsilon_0 \cdot \left(\varepsilon_r^{'} - i \varepsilon_r^{''} \right) \tag{2.8}$$

where ε_r^* is the complex relative permittivity, $\varepsilon_r^{'}$ is the relative dielectric constant, and $\varepsilon_r^{''}$ is the loss factor. The relative dielectric constant indicates the ability of a material to store energy in an electric field (relative to that of free space), while the loss factor indicates the ability of the material to absorb electromagnetic energy [5].

In case of applying an alternating electric field to a dipole, the dipole rotates to align itself with the field. As it rotates, a fraction of electromagnetic energy is lost through the generation of heat (friction) as well as the acceleration and deceleration of the rotational motion of the dipole. The amount of loss determines how large the imaginary part of the permittivity is as a function of frequency. The larger the imaginary part, the more energy is being dissipated through motion, and the less energy is available to propagate past the dipole.

The absorption of energy by the material, according to Eq. 2.6, causes a phase difference between **E** and **D**. Therefore, a dissipation factor, $tan\delta$, is defined that relates the phase difference, δ, and the components of the complex relative permittivity:

$$tan\delta = \frac{\varepsilon_r^{''}}{\varepsilon_r^{'}}. \tag{2.9}$$

The frequency where the dielectric loss is at its maximum is called dispersion or relaxation frequency, f_d. Thus, the relaxation time is defined as $\tau = \frac{1}{f_d}$.

Loss in a dielectric material may also occur due to collisions of electrons with other electrons and atoms called finite conductivity, σ. thus, the relative permittivity in Eq. 2.8 can be restated to include the conductivity loss:

$$\varepsilon_r^* = \varepsilon_r^{'} - i(\varepsilon_r^{''} + \frac{\sigma}{\omega\varepsilon_0}). \tag{2.10}$$

It is well known that the permittivity varies with frequency. The Debye equation is widely used at the microwave and lower frequencies to define this variation [6]:

$$\varepsilon_r^* = \varepsilon_\infty + \frac{\varepsilon_s - \varepsilon_\infty}{1 + j\omega\tau} - i\frac{\sigma}{\omega\varepsilon_0} \tag{2.11}$$

where ε_s is the static relative permittivity (relative permittivity at low frequencies), ε_∞ is the high frequency relative permittivity (infinite relative permittivity), ω is the angular frequency, and τ is the relaxation time [7].

In complex materials, several relaxation processes can take place. This can be described as a sum of Debye processes with different relaxation times. If the relaxation times are symmetrically distributed around a common value τ, they can be represented by introducing an empirical factor, α, in Eq. 2.11:

$$\varepsilon_r^* = \varepsilon_\infty + \frac{\varepsilon_s - \varepsilon_\infty}{1 + (j\omega\tau)^{1-\alpha}} - i\frac{\sigma}{\omega\varepsilon_0}. \tag{2.12}$$

Eq. 2.12 is called Cole-Cole equation [8], and the empirical factor, α, is called distribution factor. When the α is zero, the Cole-Cole model is equivalent to

the Debye model. The typical relative permittivty spectrum of distilled water, according to the Cole-Cole equation, is shown in Figure 2.1.

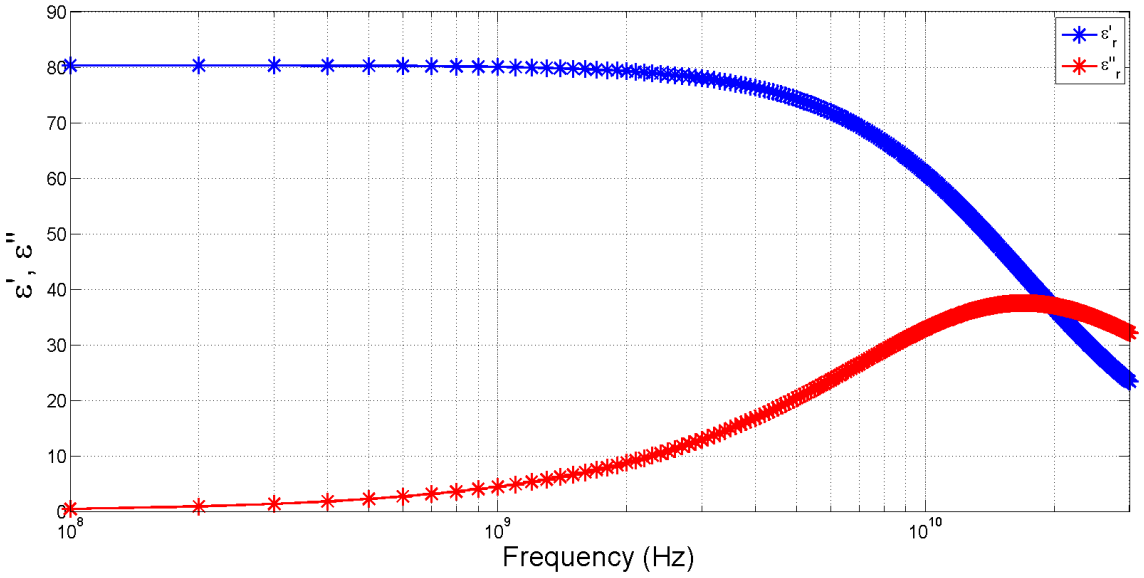

Figure 2.1: Permittivity spectrum of distilled water ($\varepsilon_s = 80.2933$, $\varepsilon_\infty = 5.2220$, $\tau = 9.3961\,[ps]$, $\sigma = 0$, and $\alpha = 0$ [9]).

Similar to the electric susceptibility and permittivity (as two electrical properties of a material), two magnetic properties are defined: magnetic susceptibility and permeability. For a linear media:

$$\mathbf{B} = \mu_0(1 + \chi_M)\mathbf{H} \tag{2.13}$$

where $\mathbf{B}$ is the magnetic filed, $\mathbf{H}$ is the auxiliary field, χ_M is the magnetic susceptibility, and μ_0 is the permeability of free space ($4\pi \times 10^{-7}\, N/A^2$). μ^* is defined as $\mu_0(1 + \chi_M)$ and called permeability of the material which is a complex value. Thus:

$$\mathbf{B} = \mu^*\mathbf{H}. \tag{2.14}$$

2.1.3 Propagation of Electromagnetic Waves in Waveguides

RF (Radio Frequency) waveguides are used in a variety of applications to carry radio frequency energy from one point to another. In the broadest term, they can be described as a system of material that is designed to confine electromagnetic waves in a direction defined by its physical boundaries. Electromagnetic waves

propagating in open space travel out in all directions and can be thought of as spherical waves emitted from a central source. As a result, the power intensity of the waves decreases as the distance increases and it is proportional to the power of the source divided by the square of the distance from the source. By contrast, the waveguide operates by confining the electromagnetic waves so that they do not spread out, and losses resulting from this effect are eliminated.

2.1.3.1 Types of RF waveguide

Figure 2.2 shows a number of different types of RF waveguides:

- **Rectangular waveguide:** This is the most commonly used form of waveguides and has a rectangular cross section.

- **Circular waveguide:** This kind of waveguides has a circular cross section.

- **Circuit board strip-line:** This form of waveguides is used on printed circuit boards as a transmission line for the microwave signals. It typically consists of a line of a given thickness above an earth plane. Its thickness defines the impedance.

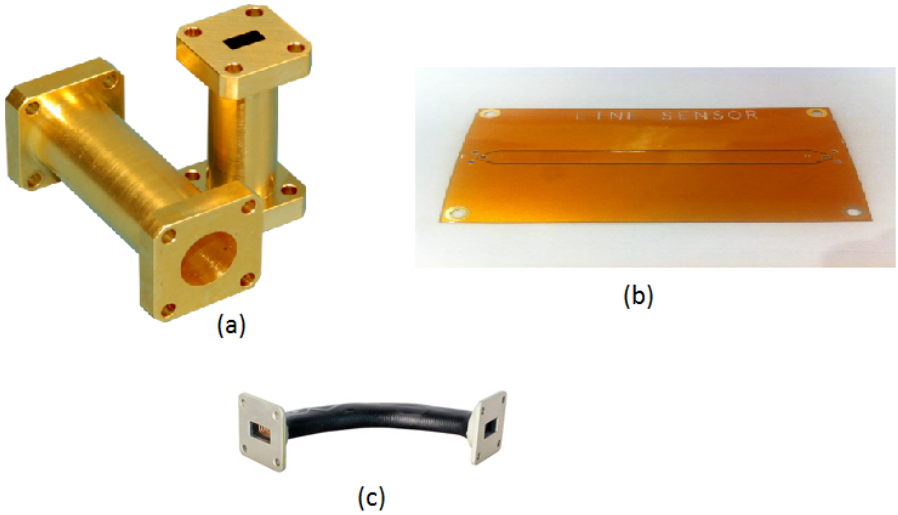

Figure 2.2: Different types of waveguide sensors: (a) rectangular and circular waveguide, (b) coplanar waveguide, (c) flexible waveguide [10],[11].

In addition to the above basic types, there are also flexible waveguides which are most widely seen in the rectangular format [12]. The waveguide theory is based on the electromagnetic wave theory and the waves is constrained, typically, within a hollow metal tube.

2.1.3.2 Waveguide theory

Assuming electromagnetic waves confined to the interior of a perfect conductor hollow pipe or waveguide (Figure 2.3), the electric field **E** and magnetic field **B** are zero inside the material itself, and the boundary conditions at the inner wall are:

$$\begin{aligned} \mathbf{E}^{\parallel} &= 0 \\ \mathbf{B}^{\perp} &= 0. \end{aligned} \tag{2.15}$$

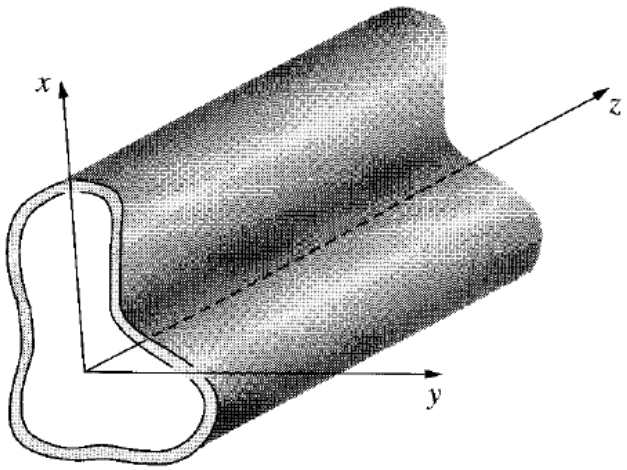

Figure 2.3: A schematic drawing of a hollow waveguide [5].

Considering monochromatic waves that propagate down the wavequide (in z direction according to Figure 2.3), **E** and **B** have the generic form:

$$\begin{aligned} \widetilde{\mathbf{E}}(x,y,z,t) &= \widetilde{\mathbf{E}}_0(x,y)e^{i(kz-wt)} \\ \widetilde{\mathbf{B}}(x,y,z,t) &= \widetilde{\mathbf{B}}_0(x,y)e^{i(kz-wt)}. \end{aligned} \tag{2.16}$$

In Eq. 2.16, $\widetilde{\mathbf{E}}_0$ and $\widetilde{\mathbf{B}}_0$ are the complex amplitudes (the physical fields are the real parts of $\widetilde{\mathbf{E}}$ and $\widetilde{\mathbf{B}}$). k is the wave number and it is related to the wavelength, λ, by the equation $\lambda = 2\pi/k$. ω is the angular frequency and is related to the frequency, f, and wave number by:

$$\omega = 2\pi f = kv \tag{2.17}$$

where v is the velocity of the wave propagation.

The electric and magnetic fields must satisfy Maxwell's equations in the interior of the waveguide:

$$
\begin{aligned}
(i)\ \nabla.\mathbf{E} = 0, \quad (iii)\ \nabla \times \mathbf{E} = -\frac{\partial \mathbf{B}}{\partial t}, \\
(ii)\ \nabla.\mathbf{B} = 0, \quad (iv)\ \nabla \times \mathbf{B} = \frac{1}{c^2}\frac{\partial \mathbf{E}}{\partial t}
\end{aligned}
\tag{2.18}
$$

where c is the velocity of light ($c = \frac{1}{\sqrt{\varepsilon_0 \mu_0}}$). The problem, then, is to find functions $\widetilde{\mathbf{E}}_0$ and $\widetilde{\mathbf{B}}_0$ such that the fields (Eq. 2.16) obey the differential equations (Eq. 2.18), subject to the boundary conditions (Eq. 2.15).

Confined waves are not in general transverse (i.e. oscillations are not necessarily perpendicular to the direction of the wave propagation). In order to fit the boundary conditions, longitudinal components (E_z and B_z) must be included:

$$
\begin{aligned}
\widetilde{\mathbf{E}}_0 = E_x\widehat{x} + E_y\widehat{y} + E_z\widehat{z}, \\
\widetilde{\mathbf{B}}_0 = B_x\widehat{x} + B_y\widehat{y} + B_z\widehat{z}
\end{aligned}
\tag{2.19}
$$

where each of the components is a function of x and y. Putting this into Maxwell's equations (iii) and (iv) results in:

$$
\begin{aligned}
(i)\ \frac{\partial E_y}{\partial x} - \frac{\partial E_x}{\partial y} = i\omega B_z, \quad (iv)\ \frac{\partial B_y}{\partial x} - \frac{\partial B_x}{\partial y} = -\frac{i\omega}{c^2}E_z, \\
(ii)\ \frac{\partial E_z}{\partial y} - ikE_y = i\omega B_x, \quad (v)\ \frac{\partial B_z}{\partial y} - ikB_y = -\frac{i\omega}{c^2}E_x, \\
(iii)\ ikE_x - \frac{\partial E_z}{\partial x} = i\omega B_y, \quad (vi)\ ikB_x - \frac{\partial B_z}{\partial x} = -\frac{i\omega}{c^2}E_y.
\end{aligned}
\tag{2.20}
$$

From Eq. 2.20(ii), (iii), (v), and (vi):

$$
\begin{aligned}
(i)\ E_x = \frac{i}{(\omega/c)^2 - k^2}(k\frac{\partial E_z}{\partial x} + \omega\frac{\partial B_z}{\partial y}), \\
(ii)\ E_y = \frac{i}{(\omega/c)^2 - k^2}(k\frac{\partial E_z}{\partial y} - \omega\frac{\partial B_z}{\partial x}), \\
(iii)\ B_x = \frac{i}{(\omega/c)^2 - k^2}(k\frac{\partial B_z}{\partial x} - \frac{\omega}{c^2}\frac{\partial E_z}{\partial y}), \\
(iv)\ B_y = \frac{i}{(\omega/c)^2 - k^2}(k\frac{\partial B_z}{\partial y} + \frac{\omega}{c^2}\frac{\partial E_z}{\partial x}).
\end{aligned}
\tag{2.21}
$$

Then, it suffices to determine the longitudinal components E_z and B_z and all the others can be calculated just by differentiating. Inserting Eq. 2.21 into the remaining Maxwell's equations yields uncoupled equations for E_z and B_z:

$$
\begin{aligned}
(i)\ [\frac{\partial^2}{\partial x^2} + \frac{\partial^2}{\partial y^2} + (\omega/c)^2 - k^2]E_z = 0, \\
(ii)\ [\frac{\partial^2}{\partial x^2} + \frac{\partial^2}{\partial y^2} + (\omega/c)^2 - k^2]B_z = 0.
\end{aligned}
\tag{2.22}
$$

If $E_z = 0$, they are called TE (Transverse Electric) waves or H waves and are characterized by the fact that the electric vector (**E**) is always perpendicular to the direction of the propagation. If $B_z = 0$, they are called TM (Transverse Magnetic) waves or E waves and are characterized by the fact that the magnetic vector (**H** or **B**) is always perpendicular to the direction of the propagation. If both $E_z = 0$ and $B_z = 0$, they are called TEM (Transverse Electric and Magnetic) waves. The TEM waves cannot be propagated within a waveguide. This is the common mode used within coaxial cables. The TEM waves are characterized by the fact that both the electric vector and the magnetic vector are perpendicular to the direction of the propagation.

Text about the waveguide theory often refers to the TE and TM waves with integers after them: TE_{mn} or TM_{mn}. The numerals m and n are always integers that can take on separate values from 0 or 1 to infinity. These indicate the wave modes within the waveguide. m indicates the number of half-wavelength variations of EM fields in the larger dimension of the waveguide opening and n shows the number of half-wavelength variations of EM fields in the other direction. Figure 2.4 shows a schematic view of the TE and TM modes inside the rectangular waveguide.

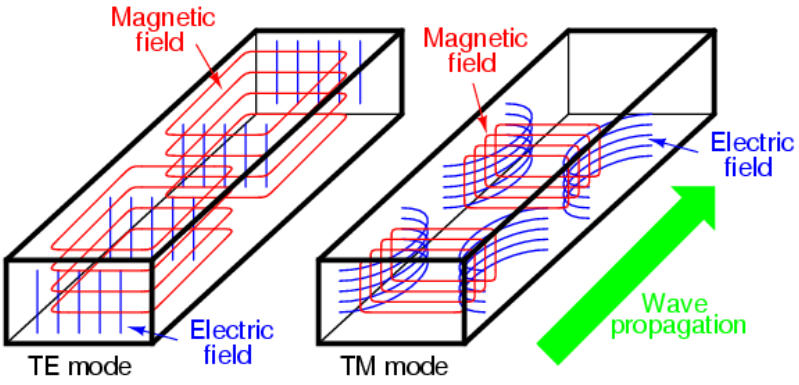

Figure 2.4: A schematic view of the TE and TM modes inside a rectangular waveguide [13].

Only a limited number of different mn modes can be propagated along a waveguide dependent upon the waveguide dimensions and format. For each mode, there is a definite lower frequency limit. This is known as the cutoff frequency. Below this frequency no signal can propagate along the waveguide. As a result, the waveguide can be seen as a high pass filter. It is also worth noting that there is only one possible mode, called dominant mode, for the lowest frequency that can be transmitted. The TE waves and the cutoff frequency of the waveguide sensor are explained in details below.

2.1.3.3 TE waves in a rectangular waveguide

A rectangular waveguide with width a and length b is shown in Figure 2.5.

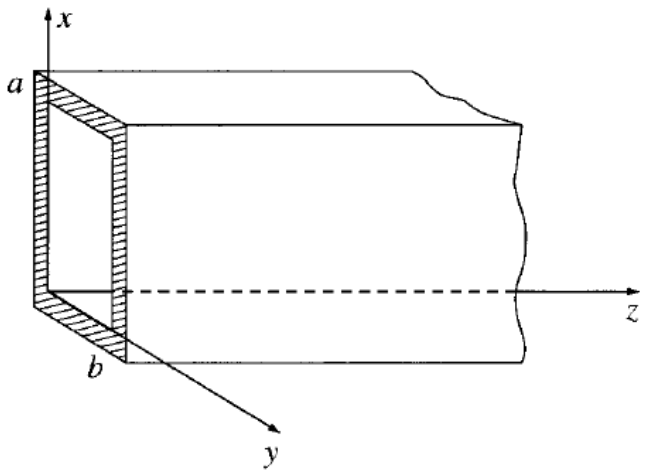

Figure 2.5: A schematic drawing of a rectangular waveguide [5].

Assuming TE waves, the problem is to solve Eq. 2.22(ii) subject to the boundary conditions of Eq. 2.15, which can be done by separating the variables:

$$B_z(x, y) = X(x)Y(y). \tag{2.23}$$

Substituting Eq. 2.23 into Eq. 2.22 gives:

$$Y\frac{d^2X}{dx^2} + X\frac{d^2Y}{dy^2} + [(\omega/c)^2 - k^2]XY = 0. \tag{2.24}$$

Dividing by XY and noting that the x- and y- dependent terms must be constant:

$$(i)\ \frac{1}{X}\frac{d^2X}{dx^2} = -k_x^2, \quad (ii)\ \frac{1}{Y}\frac{d^2Y}{dy^2} = -k_y^2. \tag{2.25}$$

Therefore, Eq. 2.24 can be restated as:

$$-k_x^2 - k_y^2 + (\omega/c)^2 - k^2 = 0. \tag{2.26}$$

The general solution to Eq. 2.25(i) is:

$$X(x) = Asin(k_x x) + Bcos(k_x x). \tag{2.27}$$

But the boundary conditions require that B_x (and also from Eq. 2.21, dX/dx) vanishes at $x = 0$ and $x = a$. Thus, $A = 0$ and:

$$k_x = \frac{m\pi}{a},\ (m = 0, 1, 2, ...). \tag{2.28}$$

The same goes for Y with:

$$k_y = \frac{n\pi}{b},\ (n = 0, 1, 2, ...) \tag{2.29}$$

and it is concluded that

$$B_z = B_0 cos(\frac{m\pi x}{a}) cos(\frac{n\pi y}{b}). \tag{2.30}$$

This solution is called TE_{mn} mode (where the first index is conventionally associated with the larger dimension of the waveguide, and therefore it is assumed that $a \geq b$). The wave number, k, is obtained by putting Eqs. 2.28 and 2.29 into Eq. 2.26:

$$k = \sqrt{(\frac{\omega}{c})^2 - \pi^2[(\frac{m}{a})^2 + (\frac{n}{b})^2]}. \tag{2.31}$$

If:

$$\begin{aligned} \omega &< c\pi\sqrt{(\frac{m}{a})^2 + (\frac{n}{b})^2} \\ f &< \frac{c}{2}\sqrt{(\frac{m}{a})^2 + (\frac{n}{b})^2} \equiv f_{mn} \end{aligned} \tag{2.32}$$

the wave number is imaginary and electromagnetic fields attenuated exponentially. f_{mn} is called cutoff frequency for the mode in question. Eq. 2.32 gives the cut-off frequency of an empty waveguide. If the waveguide is filled with a dielectric material, the cutoff frequency is calculated from:

$$f_{mn} \equiv \frac{c}{2\sqrt{\varepsilon_r^{'}\mu_r^{'}}}\sqrt{(\frac{m}{a})^2 + (\frac{n}{b})^2} \tag{2.33}$$

where $\varepsilon_r^{'}$ and $\mu_r^{'}$ are the real parts of the relative permittivity and permeability of the interior material, respectively.

In the case of m=1 and n=0, the mode is called TE_{10} mode, which is the dominant mode in the rectangular waveguides (Figure 2.6). The lowest cutoff frequency for a given waveguide occurs at this mode:

$$f_{10} = \frac{c}{2\sqrt{\varepsilon_r^{'}\mu_r^{'}}a}. \tag{2.34}$$

As mentioned before, for frequencies less than f_{10}, no wave propagates in the waveguide.

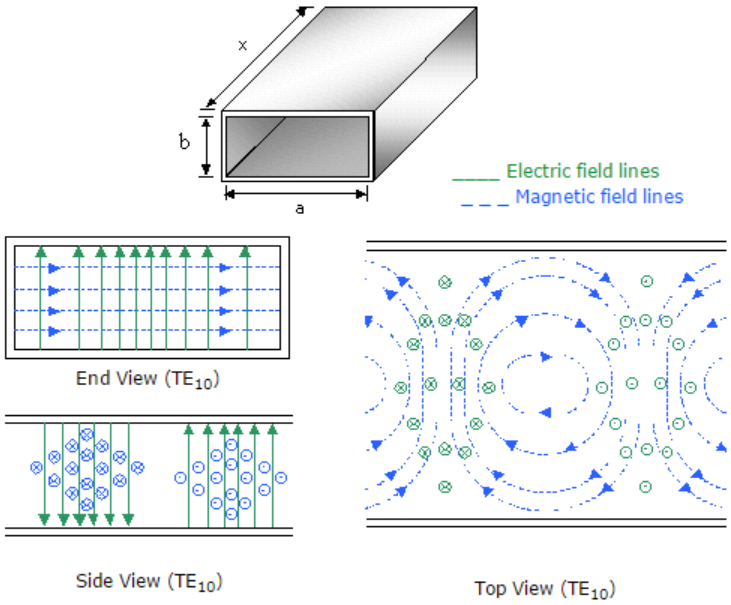

Figure 2.6: The electric and magnetic field distribution in the TE_{10} mode in the rectangular waveguide [13].

The propagation constant of the wave is an important parameter as well, which is typically shown by γ and defined as:

$$\begin{aligned}\gamma &= \frac{2\pi}{\lambda_{mn}}\sqrt{\varepsilon_r^*\mu_r^*}\sqrt{1-(\frac{f}{f_{mn}})^2} \\ &= \frac{2\pi f_{mn}}{c}\sqrt{\varepsilon_r^*\mu_r^*}\sqrt{1-(\frac{f}{f_{mn}})^2}\end{aligned} \tag{2.35}$$

where λ_{mn} is the cutoff wavelength, ε_r^* is the relative permittivity, and μ_r^* is the relative permeability of the interior material. γ is a complex parameter and restated as $\alpha + j\beta$, where α and β are the attenuation constant and the phase constant of the wave, respectively. In case of an empty waveguide, when $f > f_{mn}$, γ is purely imaginary and there is no attenuation:

$$\gamma = \frac{2\pi f_{mn}}{c}\sqrt{1-(\frac{f}{f_{mn}})^2} = i\frac{2\pi f}{c}\sqrt{1-(\frac{f_{mn}}{f})^2}. \tag{2.36}$$

When $f < f_{mn}$, γ is purely real:

$$\gamma = \frac{2\pi f_{mn}}{c}\sqrt{1-(\frac{f}{f_{mn}})^2}. \tag{2.37}$$

This means that the phase constant is zero, and the mode is non-propagating or evanescent.

γ can be calculated for the wave propagation through the MUT layer as well. Therefore, Eq. 2.35 can be restated as:

$$\begin{aligned}\gamma &= \frac{2\pi f_{mn}}{c}\sqrt{\varepsilon_r^*\mu_r^*}\sqrt{1-(\frac{f}{f_{mn}})^2} \\ &= \frac{2\pi}{c}\sqrt{\varepsilon_r^*\mu_r^*}\sqrt{f_{mn}^2-f^2} \\ &= \frac{2\pi f}{c}\sqrt{\varepsilon_r^*\mu_r^*}\sqrt{(\frac{f_{mn}}{f})^2-1} \\ &= \frac{\omega}{c}\sqrt{\varepsilon_r^*\mu_r^*}\sqrt{(\frac{f_{mn}}{f})^2-1}\end{aligned} \tag{2.38}$$

where ε_r^* and μ_r^* are the relative permittivity and relative permeability of the MUT layer, respectively. In this case, the wave is not bounded and f_{mn} is approximately zero. Assuming $\mu_r^* = 1$:

$$\gamma = i\frac{\omega}{c}\sqrt{\varepsilon_r^*}\ . \tag{2.39}$$

For a loss-less MUT ($\varepsilon_r^{''} = 0$), γ is purely imaginary, and therefore the attenuation constant will be zero.

2.1.4 Scattering Parameters

Scattering parameters or briefly S-parameters can be explained most easily by first considering a two-port network with incident and reflected waves at the input, and transmitted and load reflected waves at the output. According to Figure 2.7, if a_1 and a_2 are defined as waves entering, and b_1 and b_2 are defined as waves leaving the network [14],[15]:

$$\begin{aligned}b_1 &= S_{11}a_1 + S_{12}a_2, \\ b_2 &= S_{21}a_1 + S_{22}a_2\end{aligned} \tag{2.40}$$

or in matrix form:

$$\begin{pmatrix}b_1\\b_2\end{pmatrix} = \begin{pmatrix}S_{11} & S_{12}\\S_{21} & S_{22}\end{pmatrix}\begin{pmatrix}a_1\\a_2\end{pmatrix}\ . \tag{2.41}$$

Since the waves have amplitude and phase, the S-parameters are complex values. The S-parameters can be expressed as wave ratios by placing a matched load on each port in turn. Thus, for a matched load on port 2, $a_2 = 0$ and:

$$S_{11} = \frac{b_1}{a_1}, \quad S_{21} = \frac{b_2}{a_1}. \tag{2.42}$$

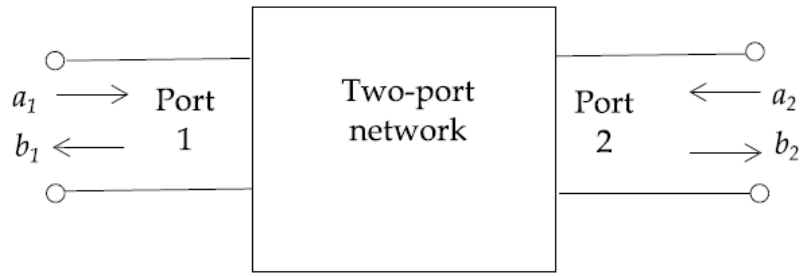

Figure 2.7: Definition of the input and output ports in a two-port network [14].

Similarly for a matched load on port 1, $a_1 = 0$ and:

$$S_{22} = \frac{b_2}{a_2}, \quad S_{12} = \frac{b_1}{a_2}. \tag{2.43}$$

S_{11} and S_{22} are called reflection coefficients at the ports and S_{12} and S_{21} are called transmission coefficients through the network [14].

2.2 Permittivity Measurement Techniques

A number of techniques have been developed to determine the relative permittivity of materials. Measurement methods relevant for any desired application depend on the nature of the dielectric material to be measured, both physically and electrically, the frequency of interest, and the degree of accuracy required. These techniques can be categorized in different ways; for example destructive vs. non-destructive methods, single vs. broadband methods, resonant vs. non-resonant methods, and reflection vs. transmission methods. Each technique is accompanied by some advantages and disadvantages, for instance although single frequency methods ensure high accuracy permittivity measurements, they are rather time consuming methods. In contrast, broadband methods provide quicker permittivity measurements over a wide frequency range; however, they are less accurate.

Dielectric property (permittivity) measurement methods range from low frequency capacitive methods to high frequency microwave techniques. At low frequencies (i.e. below approximately 10 MHz), parallel plates and coaxial capacitors are commonly used to estimate the permittivity of a sample by placing the sample in the capacitor and then measuring the admittance of the cell with an impedance bridge [16]. Through a master project at Christian Michelsen Research (CMR), the feasibility of using the capacitance sensing technique to monitor the formation

of gas hydrates was investigated [17]. In that research, the temperature and capacitance of two hydrate-forming test-samples with different water fractions were measured in the kHz frequency range. The measured capacitance data was then used to find the permittivity information of the sample using capacitance sensor calibration curves. By following the measured permittivity and temperature variations of the hydrate-forming samples as a function of time, it was shown that the information derived from the capacitance sensor could be an indication of different stages of the hydrate generation and evolution.

At higher frequencies (the microwave frequencies, below approximately 10 GHz), transmission line, resonant cavity, and free-space methods are commonly used for measuring the permittivity [18].

In general, permittivity measurement techniques at the microwave frequencies can be categorized as reflection or transmission type, using resonant or non-resonant systems, with open or closed structures [18]. A brief explanation of different permittivity measurement methods at high frequencies are explained below.

2.2.1 Non-resonant Methods

In non-resonant methods, the properties of material are fundamentally deduced from its impedance and wave velocity therein. When an electromagnetic wave propagates from one material to another, both the characteristic impedance and the wave velocity change, resulting in a partial reflection of the wave from the interface between the two materials. Measurements of the reflection from such an interface and the transmission through it, can provide information about the permittivity and permeability relationships between the two materials. Non-resonant methods mainly include reflection and reflection/transmission methods.

In a reflection method, the properties of the MUT are deduced from the magnitude and phase measurement of the reflected signals. Two types of reflections are often used in material property characterization: open-ended reflection and short-ended reflection [15]. Figure 2.8 shows these two types for the rectangular waveguide sensor.

In a reflection/transmission method, the MUT is inserted in a piece of transmission line, and the properties of the material are deduced on the basis of the reflection from the material and the transmission through the material. For this purpose, any type of transmission line could be used; for instance a coaxial line, a hollow metallic waveguide, a planar transmission line, and free space.

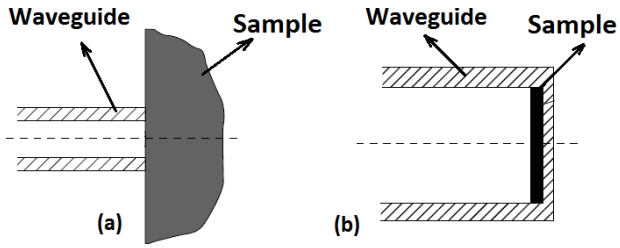

Figure 2.8: a) Open-ended reflection in a waveguide, b) short-ended reflection in a waveguide [15].

The first report of using waveguides and coaxial transmission line cells for complex permittivity measurement was published by Nicolson-Ross [19], and then by Weir [20] who analyzed the structure in the time and frequency domains. The technique involved placing an unknown sample in a microwave TEM mode fixture (more information about TEM mode in Section 2.1.3.2) and exciting the sample with a sub-nanosecond baseband pulse. The fixture was used to measure the transmission and reflection coefficients, S_{21} and S_{11}, respectively. It was shown that S_{11} and S_{21} are uniquely related to the intrinsic properties of the materials, namely ε_r^* and μ_r^* [18].

Folgerø et. al. used coaxial measurement cells for a broad band permittivity measurement of low-permittivity fluids in the frequency domain [21]. Due to different measurement techniques and different measurement cells, the frequency range was divided into three sub-ranges. In the lowest frequency range (1 kHz to 5 MHz), the admittance of the low frequency coaxial cell was measured using an impedance analyzer. In the intermediate frequency range (10–100 MHz), the reflection coefficient was measured for the same cell by means of a network analyzer. In the highest frequency range (500 MHz to 5 GHz), the reflection coefficient was measured for a shorter coaxial cell using the network analyzer.

Folgerø later showed that the permittivity information of low-loss liquids can be measured using one single coaxial reflection/transmission cell over a broad frequency range [22]. Use of a single cell ensured that the whole dielectric spectrum was measured under the same conditions. The sensitivity of the system at frequencies above 100 MHz was increased as well.

Jakobsen and Folgerø used a time domain system for the permittivity measurement of emulsions [4]. The permittivity was calculated with a simple admittance model from the reflection coefficient measurements in the frequency range 10 MHz–10 GHz with two different open-ended coaxial probes. They showed that the gas

hydrate formation in water/oil emulsions can be monitored by permittivity measurement using open-ended probes. A simple admittance model of the probe was used to calculate the permittivity from the measured reflection coefficients.

In case of an open-ended coaxial probe, the energy is not deeply transmitted into the environment in front of the probe, and therefore it is considered as a near surface sensor with limited penetration capability [7],[23].

In two other research projects at CMR, the characteristics of the coplanar waveguide as a non-intrusive permittivity sensor was studied [10],[24]. The sensor was used in sensing of hydrocarbon non-uniform thin layers close to the pipe wall surface.

The free space technique is also grouped under non-resonant methods. It is a non-destructive and contact-less permittivity measurement method which is generally employed at frequencies above 10 GHz. In a typical free space transmission measurement technique, a sample is placed between two antennas (transmitter and receiver). The attenuation and phase shift of the signal are measured, from which, the dielectric properties of the sample can be estimated [25].

2.2.2 Resonant Methods

Unlike non-resonant methods (which are used in broadband frequency range), resonant methods usually offer the potential of characterizing the properties of a material at a single frequency or a discrete set of frequencies. Therefore, they normally have higher accuracies and sensitivities than non-resonant methods, and they are most suitable for low-loss samples. Resonant methods generally include the resonator method and the resonant-perturbation method. The resonator method is based on the fact that the resonant frequency and quality factor of a dielectric resonator with given dimensions are determined by its permittivity and permeability. The resonant-perturbation method is based on the resonant perturbation theory. For a resonator with given electromagnetic boundaries, when one part of the electromagnetic boundary condition is changed by introducing a sample, its resonant frequency and quality factor will also change. From the changes of the resonant frequency and quality factor, the dielectric properties of the sample can be derived [15]. Some applications of resonant methods for dielectric property characterization of materials have been explained in [26],[27].

2.3 Permittivity and Thickness Estimation Method

The main aim of this project was to estimate the relative permittivity and thickness of dielectric materials. This target was achieved through the reflection coefficient measurement method using a rectangular open-ended waveguide sensor. The difference in impedance between the waveguide and the MUT introduces signal reflections at their interface. The reflected signal was used for estimating the relative permittivity and thickness of the MUT. The steps of the estimation procedure are:

1. A simulation model of the experimental setup was developed using COMSOL multiphysics in order to achieve the following goals:

    - To calibrate the waveguide sensor in the experimental setup: Figure 2.9 depicts the interface between the waveguide, coaxial cable, and MUT container. In the experimental setup, the network analyzer was calibrated at the end of the coaxial cable which is called "measurement plane". However, in the simulation model, the reflection coefficients were calculated at the "simulation plane" as shown in Figure 2.9. There was an N type connector between the end of the coaxial cable (the measurement plane) and the waveguide opening (the simulation plane). Due to internal reflections inside the connector, the results at the measurement plane had to be calibrated and transformed to the simulation plane called "transformed reflection coefficients".
    - To generate permittivity and thickness lookup matrices: The permittivity lookup matrix gives the simulated reflection coefficient as a function of frequency and relative permittivity for a specific thickness. The thickness lookup matrix provides the simulated reflection coefficient as a function of frequency and thickness for a specific relative permittivity (see Section 3.3).

2. The reflection coefficient for specific fluids with known relative permittivity and thickness was measured to calibrate the waveguide sensor. Using the COMSOL simulation model, the reflection coefficient for the corresponding fluids was calculated, too. A bilinear transformation was introduced to map the measurement results to the corresponding simulation results (see Section 3.2). This transformation was used to calibrate all measured reflection coefficients.

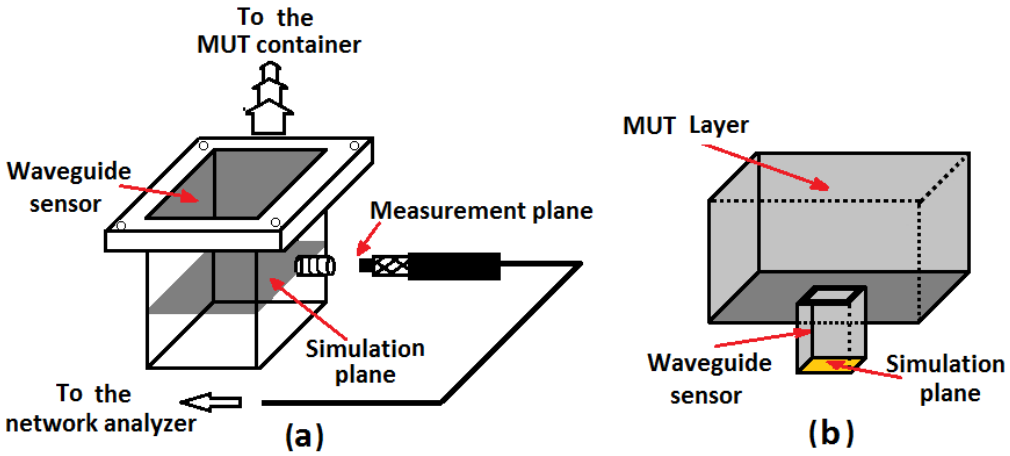

Figure 2.9: (a) The interface between the coaxial cable and the waveguide which is defined as measurement plane, (b) A schematic drawing of the COMSOL simulation model. The simulation plane is defined as a plane inside the waveguide, perpendicular to the axial direction of the waveguide.

3. The permittivity and thickness lookup matrices were used to estimate the relative permittivity and thickness from the transformed reflection coefficient:

   - In the case of relative permittivity estimation, at each frequency, the absolute deviation between the transformed reflection coefficient and each element of the permittivity lookup matrix was calculated. The cell with the minimum deviation represented the estimated relative permittivity at that frequency.
   - In the case of thickness estimation, at each frequency, the absolute deviation between the transformed reflection coefficient and each element of the thickness lookup matrix was calculated. Then, for each individual thickness value in the lookup matrix (each row), the arithmetic mean of the absolute deviations over the whole frequency range was calculated called "total deviation". The row with the minimum total deviation represented the estimated thickness.

4. Finally, the above methodology was verified. Using the experimental setup, the reflection coefficient for a set of MUTs with known relative permittivity and thickness was measured and transformed to the transformed reflection coefficient. The relative permittivity and thickness were estimated using the lookup matrices, and the results were compared with the actual values.

Chapter 3

Simulation

In this chapter the COMSOL simulation model of the experimental setup is presented. This model was used to calibrate the experimental setup and to generate the permittivity and thickness lookup matrices. The matrices established a relationship between the reflection coefficient and the relative permittivity or thickness of the MUT.

3.1 COMSOL Simulation Model

3.1.1 Introduction to COMSOL Multiphysics

COMSOL multiphysics is a general-purpose software platform based on advanced numerical methods and the Finite Element Method (FEM), which is used for various physics and engineering applications. The FEM approximates solutions to the partial differential equations by dividing a complicated model into a number of smaller model elements, solving the differential equations for these smaller model elements, and finally integrating the solutions [28].

3.1.2 Model Geometry and Material

The geometry of the simulation model is shown in Figure 3.1. Due to symmetry and in order to shorten the simulation time, the simulation model was reduced in size to a one-fourth model representing the actual experimental setup. This model consists of 6 blocks which are defined in Table 3.1.

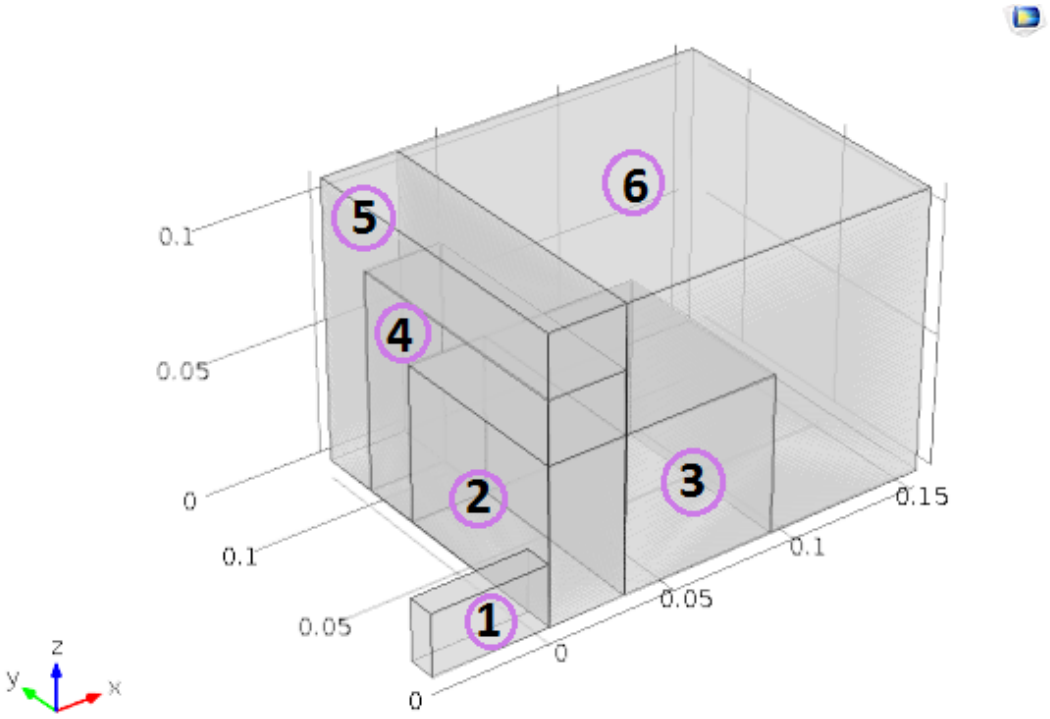

Figure 3.1: Geometry of the COMSOL simulation model.

Table 3.1: Block definition of the COMSOL simulation model.

Block No.	Definition	Interior material
1	Waveguide	Air
2	MUT	See Table 3.2
3 and 4	Backing material	Air
5 and 6	PML	Air

The MUT was air, diesel, ethanol/water mixtures or distilled water. The electrical properties of these materials are given in Table 3.2. According to the experimental setup, there was an air layer around the MUT container. In the simulation model this layer was defined as blocks 3 and 4 called backing material. Blocks 5 and 6 were defined as Perfectly Matched Layers (PML), absorbing layers for the wave equations commonly used to truncate computational regions in numerical methods to simulate problems with open boundaries in the FEM. Waves incident upon the PML from a non-PML medium do not reflect at the interface. This property allows the PML to strongly absorb outgoing waves from the interior of a computational region without reflecting them back into the interior (Figure 3.2).

Table 3.2: Electrical properties of different MUTs at $20^{\circ}C$.
(*: Applied molar fraction of ethanol in the ethanol/water mixture.)

Material under test	ε_s	ε_∞	$\tau\,[ps]$	$\sigma\,[S/m]$	α	Ref.
Air	1	1	-	0	0	[9]
Diesel	2.3	2.3	-	0	0	[7]
Ethanol/water $x_e^* = 0.76$	29.8000	5.6000	121	0	0	[29]
Ethanol/water $x_e = 0.54$	36.5000	8.1000	80	0	0	[29]
Ethanol/water $x_e = 0.36$	45.2000	10.1000	55	0	0	[29]
Distilled water	80.2933	5.2220	9.3961	0	0	[9]

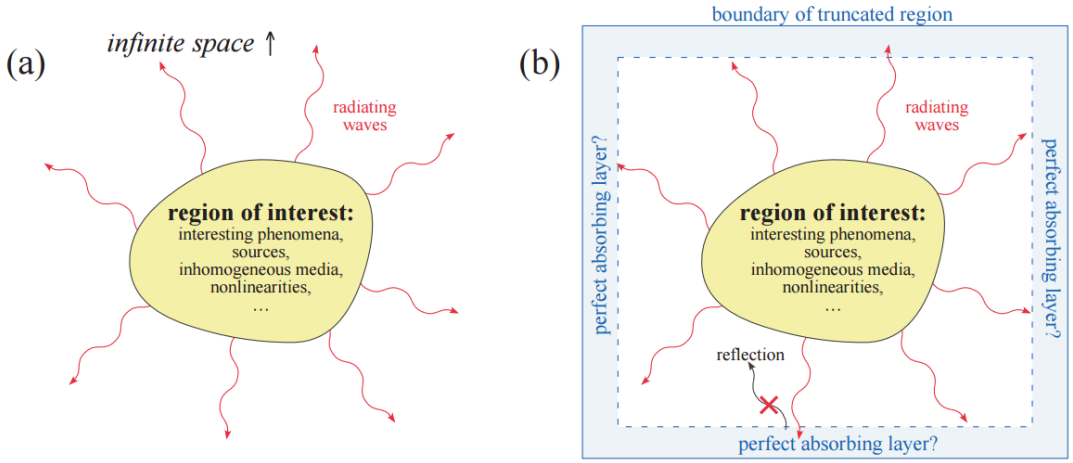

Figure 3.2: (a) Schematic of a typical wave-equation problem, in which, there is some finite region of interest from which some radiative waves escape to infinity. (b) The same problem where space has been truncated by PML [30].

Figure 3.3 shows dimension details of the blocks in the simulation model, and Table 3.3 provides the value of the parameters presented in Figure 3.3 which were related to the reduced-size model. The thickness of the backing material was chosen to be 2d; however, it could be as low as the MUT thickness (d) because there was a PML layer behind this block. The PML block led to the same reflection coefficients regardless of the backing material thickness.

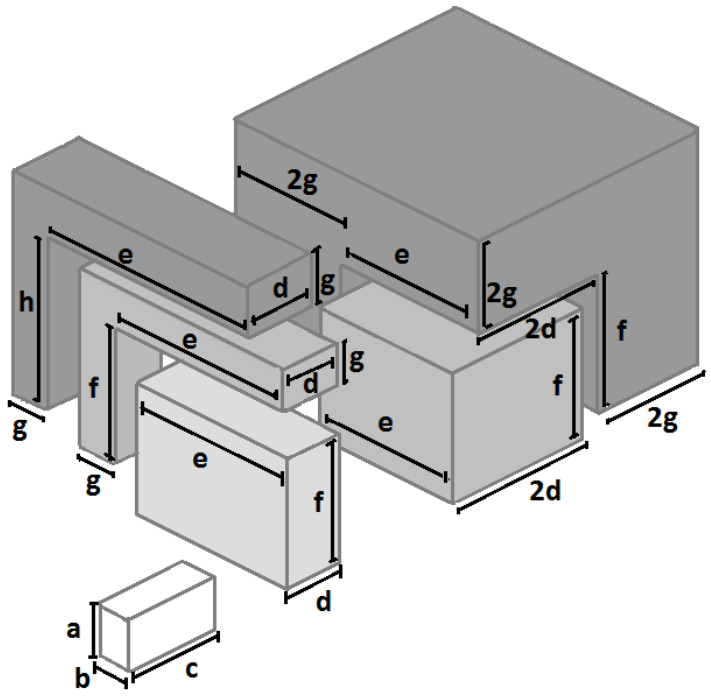

Figure 3.3: Geometrical dimensions of the COMSOL simulation model.

Table 3.3: List of the parameters defining the geometry of the COMSOL simulation model. In the simulation model the value of each parameter except "c" and "d" was 50% of the actual value in the experimental setup (due to defining a reduced-size model).

Parameter:	a	b	c	d	e	f	g	h
Value (mm):	23.75	11	45	0-30	75	60	23.75	83.75

3.1.3 Selected Physics

In this study, the COMSOL "Radio Frequency" module and "Electromagnetic Waves (EM), Frequency Domain" were used. To simulate the experimental setup more precisely, boundary conditions were added to the simulated model by defining perfect electric conductors ($\hat{\mathbf{n}} \times \mathbf{E} = \mathbf{0}$) and perfect magnetic conductors ($\hat{\mathbf{n}} \times \mathbf{H} = \mathbf{0}$, where $\hat{\mathbf{n}}$ is the normal vector of the boundary).

The port (which radiated EM waves through the waveguide) was excited by an electric field with a power of 0.25 W such that the TE_{10} mode was the dominant

mode in the simulated waveguide. Regarding the width of the waveguide ($2a$, where a was given in Table 3.3), the cutoff frequency for the TE_{10} mode was: $f_{10} = \frac{c}{2(2a)} \approx 3.16$ GHz, c is the velocity of light.

The boundary conditions and the port are illustrated in Figure 3.4.

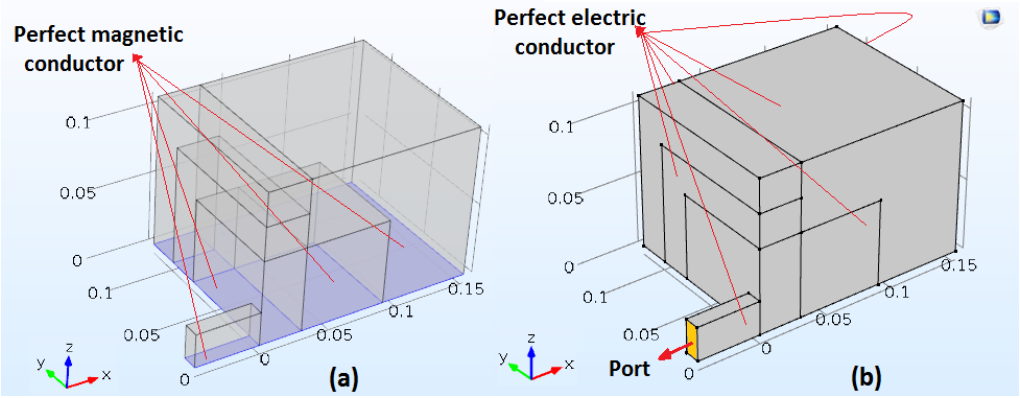

Figure 3.4: Boundary conditions in the COMSOL simulation model (all dimensions in meter). (a) Perfect magnetic conductors are shown in blue. (b) Perfect electric conductors and port are shown in gray and yellow, respectively.

3.1.4 Meshing

A free tetrahedral mesh was used for the entire simulation model, as shown in Figure 3.5. To select a suitable mesh size, a convergence analysis was performed using 3 cm of water as the MUT. The model was solved iteratively on progressively finer meshes until the difference between the last two consecutive solutions was insignificant (less than 1%). In the case of the MUT and backing layers, "extra fine" meshing; and for the PMLs, "finer" meshing from the predefined menu were selected. In the case of the waveguide, a mesh size finer than the suggested default setting was defined in order to have a more accurate result (the maximum element size was selected to be 0.003 m). Figure 3.6 shows the convergence test result. It was found that the difference between the highest mesh quality result (blue line) and the defined mesh size (red line) was insignificant, and therefore the defined mesh size was assumed to provide an acceptable resolution.

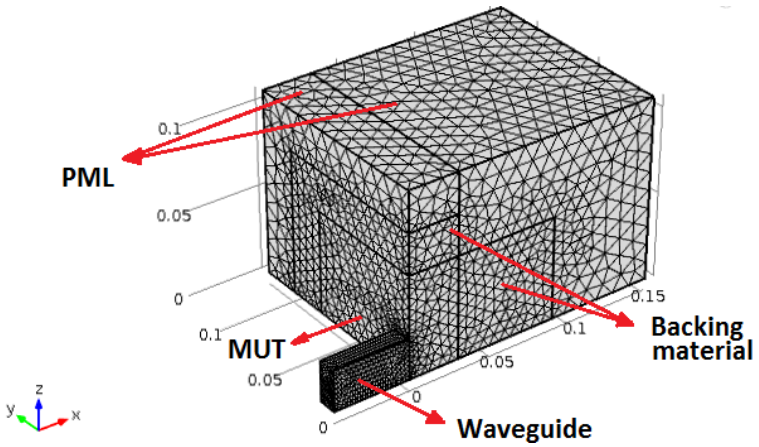

Figure 3.5: 3D mesh plot of the simulation model (dimensions in meter).

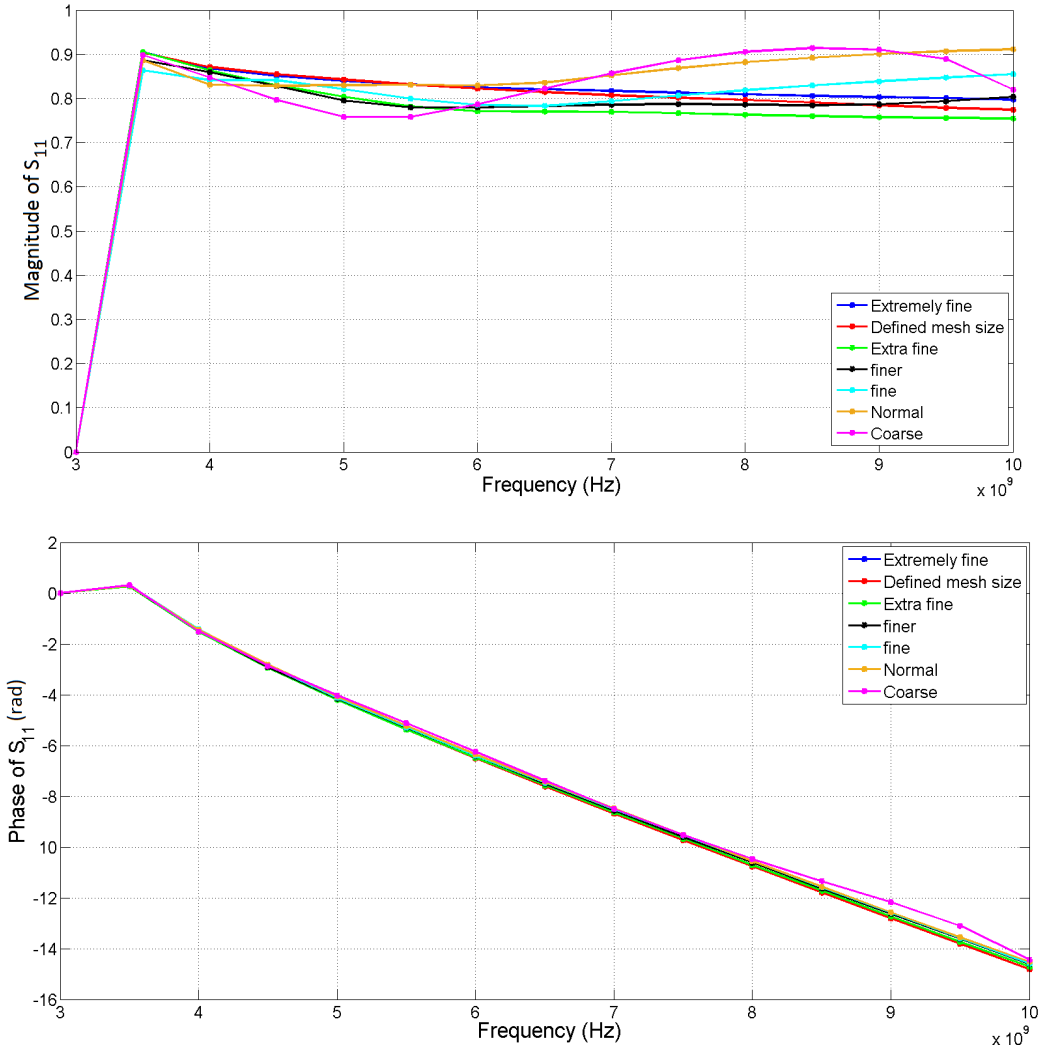

Figure 3.6: Convergence test of the simulation model as a function of different mesh resolutions for 3 cm of water.

3.2 Calibration Procedure

As it was shown previously in Figure 2.9, in the experimental setup, the network analyzer was calibrated at the end of the coaxial cable (at the measurement plane) while in the simulation model, the reflection coefficient was calculated at the simulation plane. That is because there was an N type connector between the end of the coaxial cable and the waveguide opening (the simulation plane). Due to internal reflections inside the connector, there was a phase lag between the reflection coefficient at the simulation plane and the reflection coefficient at the measurement plane. Therefore, the measured reflection coefficient at the measurement plane was calibrated and transformed to the simulation plane called "transformed reflection coefficient".

Figure 3.7 shows a two-port error network that represents the region between the measurement plane and the simulation plane. S_{11}^M and S_{11}^R are the measured and transformed reflection coefficients, respectively. Using a bilinear transformation, the measured reflection coefficient was converted to the transformed reflection coefficient [31]:

$$S_{11}^R = \frac{S_{11}^M - E_{11}}{E_{22} \cdot S_{11}^M - (E_{11} \cdot E_{22} - E_{12} \cdot E_{21})} \tag{3.1}$$

where E_{11}, E_{12}, E_{21}, and E_{22} are the scattering parameters of the error network.

Eq. 3.1 can be restated as:

$$S_{11}^R = \frac{A \cdot S_{11}^M + B}{C \cdot S_{11}^M + 1} \tag{3.2}$$

where A, B, and C are frequency dependent and complex coefficients. In order to determine these three coefficients, S_{11}^M and S_{11}^R parameters were obtained for three different fluids with known relative permittivity, using the experimental setup and the simulation model, respectively. Table 3.4 lists the required equations for calculating the coefficients.

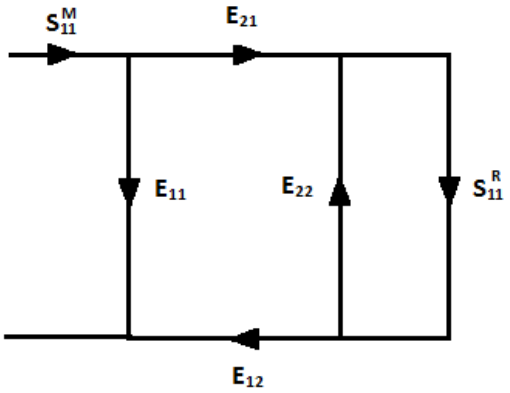

Figure 3.7: Two port error network for modeling the region between the measurement and simulation planes [7].

Table 3.4: Derived equations for calculating the A, B, and C coefficients in the bilinear transformation.

r_1:	S_{11}^R for 1st calibration fluid
r_2:	S_{11}^R for 2nd calibration fluid
r_3:	S_{11}^R for 3rd calibration fluid
m_1:	S_{11}^M for 1st calibration fluid
m_2:	S_{11}^M for 2nd calibration fluid
m_3:	S_{11}^M for 3rd calibration fluid
A=	$\frac{r_1 \cdot m_1 \cdot r_2 - r_2 \cdot m_2 \cdot r_1 + r_3 \cdot r_2 \cdot m_2 - r_3 \cdot r_1 \cdot m_1 + r_1 \cdot r_3 \cdot m_3 - r_2 \cdot r_3 \cdot m_3}{m_1 \cdot r_3 \cdot m_3 - m_2 \cdot r_3 \cdot m_3 - m_3 \cdot r_1 \cdot m_1 + m_3 \cdot r_2 \cdot m_2 - m_1 \cdot m_2 \cdot r_2 + r_1 \cdot m_1 \cdot m_2}$
B=	$\frac{A \cdot m_1 \cdot m_2 \cdot r_2 - A \cdot r_1 \cdot m_1 \cdot m_2 - r_2 \cdot m_2 \cdot r_1 + r_1 \cdot m_1 \cdot r_2}{r_1 \cdot m_1 - r_2 \cdot m_2}$
C=	$\frac{A \cdot m_1^2 \cdot r_1 - A \cdot r_1 \cdot m_1 \cdot m_2 + r_1 \cdot m_1 \cdot r_2 - r_1^2 \cdot m_1}{r_1^2 \cdot m_1^2 - r_1 \cdot m_1 \cdot r_2 \cdot m_2}$

For instance water, air, and a mixture of ethanol/water 0.76 molar ($x_e = 0.76$) were selected for the calibration procedure with electrical properties as mentioned in Table 3.2. The reflection coefficient for these fluids with a specific thickness e.g. 3 cm was obtained from the simulation model in the frequency range 3–10 GHz (in steps of 0.5 GHz). In addition, the reflection coefficient for the fluids in the frequency range 0.5–10 GHz was measured using the experimental setup explained in Chapter 4. The calculated A, B, and C coefficients are listed in Appendix A.

To validate the calibration procedure, a mixture of ethanol/water 0.36 molar ($x_e = 0.36$) with thickness of 3 cm was selected as the MUT. The magnitude and phase of the measured (S_{11}^M), transformed (S_{11}^R), and simulated reflection coefficients in the frequency range 3–10 GHz are shown in Figure 3.8. Deviation between the

transformed and simulated reflection coefficient was called calibration error and calculated from:

$$Calibration\ error = \sqrt{(\frac{Re_{sim} - Re_{trans}}{Re_{sim}})^2 + (\frac{Im_{sim} - Im_{trans}}{Im_{sim}})^2} \tag{3.3}$$

where Re_{sim} and Re_{trans} are the real parts and Im_{sim} and Im_{trans} are the imaginary parts of the simulated and the transformed reflection coefficient, respectively. It was found that in the range 4–6 GHz, the maximum and the mean value of the calibration error were 13.42% and 7.68%, respectively. Therefore, the transformed reflection coefficient followed the simulated reflection coefficient fairly good at this frequency range. However, at frequencies higher than 6 GHz, the mean value of the calibration error was 44.06% (more explanation about this behavior is given in Section 5.2).

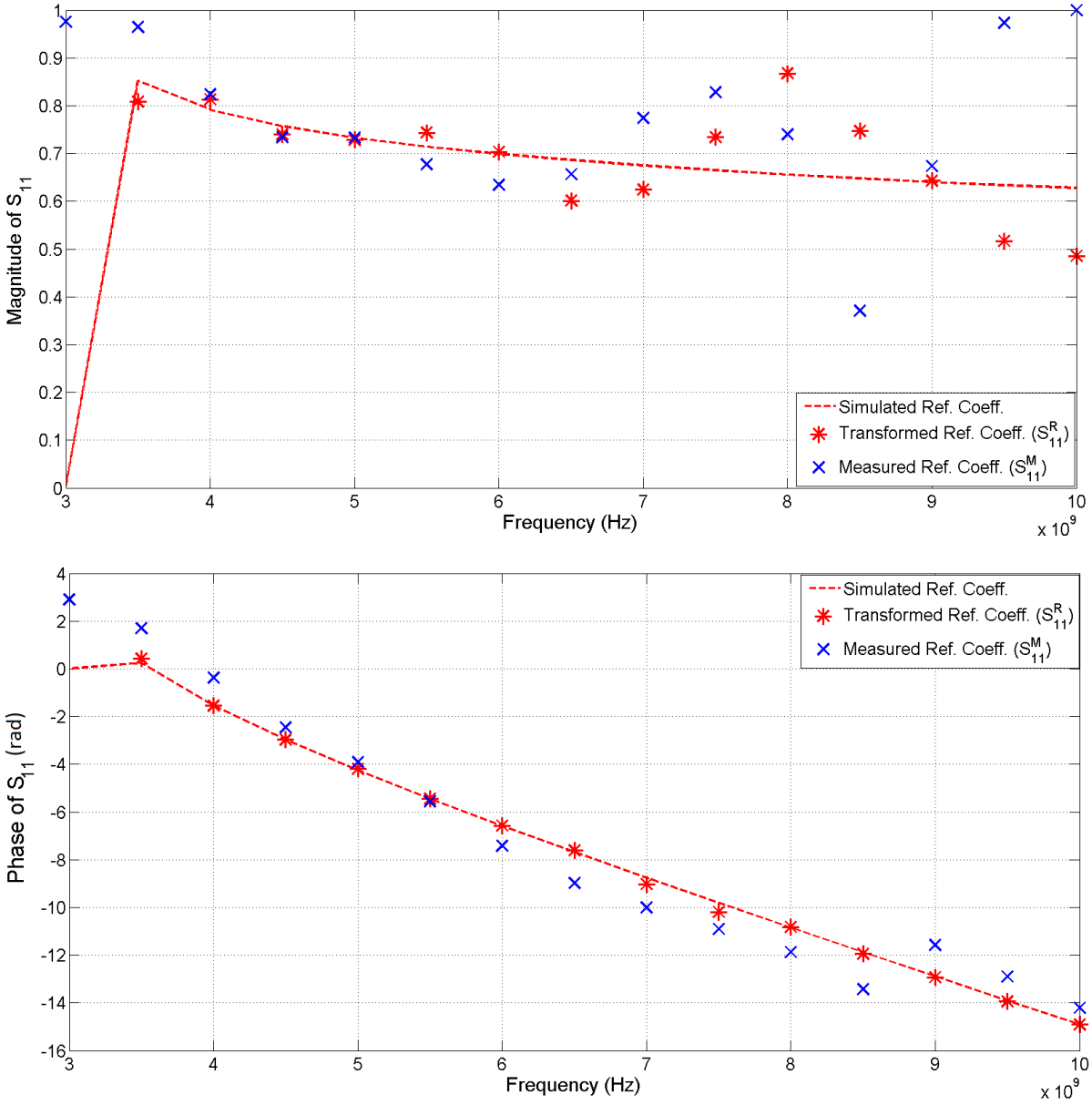

Figure 3.8: The magnitude and phase of the transformed, simulated, and measured reflection coefficients for ethanol/water 0.36 molar ($x_e = 0.36$) with a thickness of 3 cm.

3.3 Generating the Lookup Matrix

In order to relate the transformed reflection coefficient to the relative permittivity and thickness of the MUT, two lookup matrices were generated via the COMSOL simulation model:

- A permittivity lookup matrix which gives the simulated reflection coefficient for a specific MUT thickness, as a function of relative permittivity in the frequency range 3–10 GHz.
- A thickness lookup matrix which gives the simulated reflection coefficient for a specific permittivity, as a function of thickness in the frequency range 3–10 GHz.

3.3.1 Permittivity Lookup Matrix

To obtain the simulated reflection coefficients and form the permittivity lookup matrix, a 3 cm layer was defined as the MUT layer in the simulation model. By using the "parametric sweep" option of COMSOL, the real and imaginary parts of the relative permittivity ($\varepsilon_r^{'}$ and $\varepsilon_r^{''}$) were swept from 1 to 30 and 1 to 17, respectively, both in steps of 5.

To get a higher resolution in the relative permittivity estimation, it was required to expand the matrix. As the first attempt, the expansion was performed by using an interpolation technique. However, the results of the permittivity estimation using the corresponding expanded matrix was unsatisfactory. The reason is explained below:

Figure 3.9(a) shows how the magnitude of the reflection coefficient increased smoothly by increasing the dielectric constant, while the loss factor was 17. A polar plot of the reflection coefficient is shown in Figure 3.9(b) as well. As it is clear from the figures, there was not any sudden change in the reflection coefficient value in this case. On the contrary, for a low-loss MUT layer, a small change in the dielectric constant changed the corresponding reflection coefficient rapidly. Due to these rapid changes, the matrix could not be expanded properly by using an interpolation technique. Figure 3.10(a) shows how the magnitude of the reflection coefficient changed by changing the dielectric constant, while the loss factor was zero; and Figure 3.10(b) shows a polar plot of the reflection coefficient (the frequency is 5 GHz and the thickness of the MUT is 3 cm in the both figures). The sharp variations of the reflection coefficient is clear in the figures.

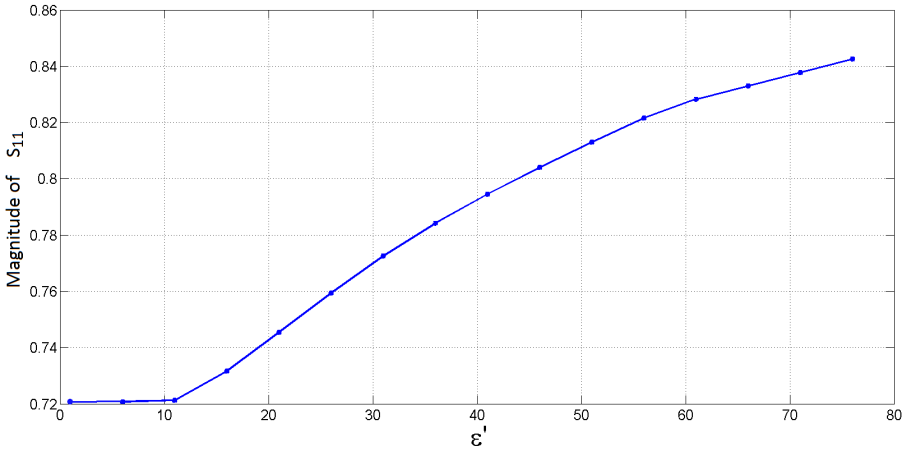

(a)

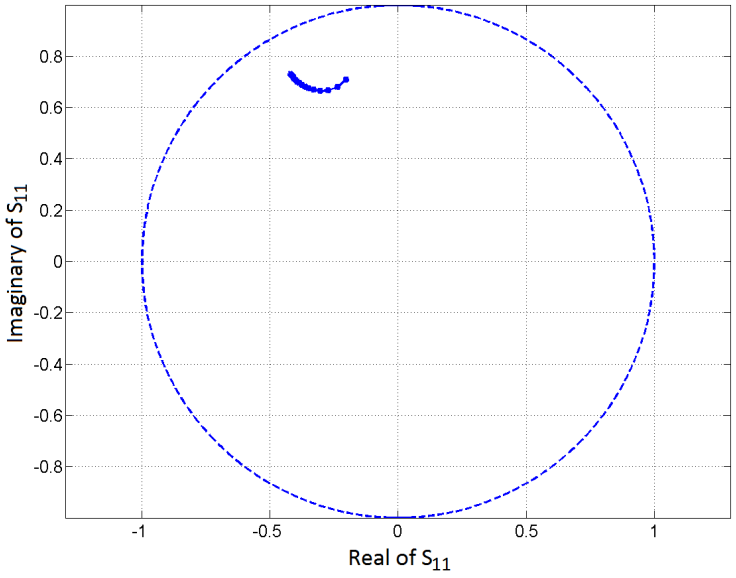

(b)

Figure 3.9: (a) The magnitude of the reflection coefficient as a function of $\varepsilon_r^{'}$ for $f = 5\,GHz$ and $\varepsilon_r^{''} = 17$ (thickness of the MUT is 3 cm). (b) Polar plot of the reflection coefficient corresponding to $1 \leq \varepsilon_r^{'} \leq 76$, for $f = 5\,GHz$ and $\varepsilon_r^{''} = 17$ (thickness of the MUT is 3 cm).

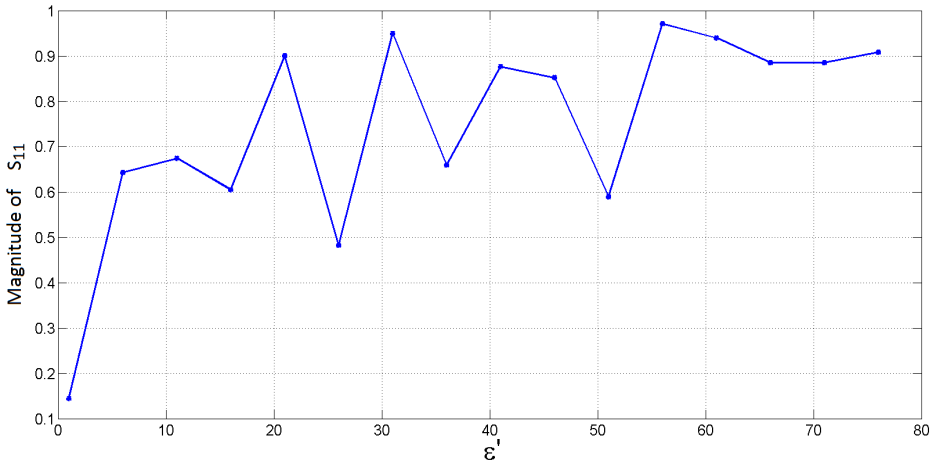

(a)

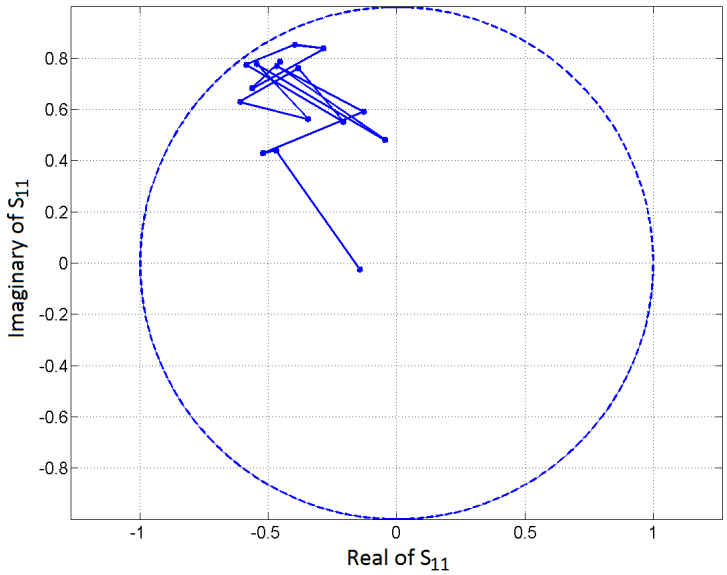

(b)

Figure 3.10: (a) The magnitude of the reflection coefficient as a function of $\varepsilon_r^{'}$ for $f = 5\,GHz$ and $\varepsilon_r^{''} = 0$ (thickness of the MUT is 3 cm). (b) Polar plot of the reflection coefficient corresponding to $1 \leq \varepsilon_r^{'} \leq 76$, for $f = 5\,GHz$ and $\varepsilon_r^{''} = 0$ (thickness of the MUT is 3 cm).

Therefore, in order to expand the size of the lookup matrix, the step value was reduced to 1 in the parametric sweep option of COMSOL and additional simulations were performed. The lookup matrix is shown in Tables 3.5 and 3.6 for a thickness of 3 cm. Elements of the tables are the real and imaginary parts of the simulated reflection coefficient, respectively, for different relative permittivity values.

According to the expanded lookup matrix, it was found that for permittivity values with low-loss factors (e.g. zero), the real and imaginary parts of the reflection coefficient still jumped up and down by changing the dielectric constant. Therefore, if a resolution better than 1 is needed, more simulations are required.

Table 3.5: The real part of the generated permittivity lookup matrix for a thickness of 3 cm (Perm: Permittivity).

Perm/Freq(GHz)	**3**	**3.5**	**4**	....	**9**	**9.5**	**10**
1-0i	0	-0.0007	-0.0088	....	0.0378	0.1483	-0.0114
1-1i	0	0.3335	-0.1230	....	0.0577	-0.0936	-0.1623
1-2i	0	0.4997	-0.1713	....	0.1643	-0.1318	-0.3067
.				....			
.				.			
.				.			
1-17i	0	0.8292	-0.1009	....	0.6192	0.0430	-0.5683
2-0i	0	0.3272	0.2503	....	0.3159	0.1090	-0.1631
2-1i	0	0.3991	0.0530	....	0.2000	0.0236	-0.1714
2-2i	0	0.5018	-0.0573	....	0.2390	-0.0305	-0.2710
.				....			
.				.			
.				.			
2-17i	0	0.8252	-0.0936	....	0.6178	0.0503	-0.5589
.				....			
.				.			
.				....			
29-0i	0	0.9274	0.3103	....	0.8061	0.0066	-0.4227
29-1i	0	0.8724	0.2055	....	0.7434	0.2025	-0.3841
29-2i	0	0.8550	0.1481	....	0.7099	0.2286	-0.3956
.				....			
.				.			
.				.			
29-17i	0	0.8310	0.0292	....	0.6982	0.2031	-0.4724
30-0i	0	0.8647	0.2191	....	0.7341	0.3783	-0.3416
30-1i	0	0.8702	0.1784	....	0.7020	0.2812	-0.4121
30-2i	0	0.8489	0.1392	....	0.6921	0.2614	-0.4142
.				....			
.				.			
.				.			
30-17i	0	0.8322	0.0309	....	0.7011	0.2055	-0.4725

Table 3.6: The imaginary part of the generated permittivity lookup matrix for a thickness of 3 cm (Perm: Permittivity).

Perm/Freq(GHz)	3	3.5	4	....	9	9.5	10
1-0i	0	0.3108	0.1298	....	0.1031	0.0428	-0.1068
1-1i	0	-0.0540	-0.1524	....	-0.1439	-0.1287	-0.0106
1-2i	0	-0.0475	-0.3406	....	-0.2578	-0.2778	-0.0387
.				....			
.				.			
.				.			
1-17i	0	0.1184	-0.7749	....	-0.3413	-0.7046	-0.4170
2-0i	0	0.1336	-0.3570	....	-0.0163	-0.1921	-0.2033
2-1i	0	0.0968	-0.2972	....	-0.0954	-0.2171	-0.1354
2-2i	0	0.0587	-0.3898	....	-0.1850	-0.3011	-0.1359
.				....			
.				.			
.				.			
2-17i	0	0.1232	-0.7715	....	-0.3316	-0.6982	-0.4197
.				....			
.				.			
.				....			
29-0i	0	0.2509	-0.8564	....	-0.2234	-0.3903	-0.7240
29-1i	0	0.2229	-0.7874	....	-0.1845	-0.5766	-0.6230
29-2i	0	0.2238	-0.7847	....	-0.1699	-0.6195	-0.5940
.				....			
.				.			
.				.			
29-17i	0	0.2211	-0.8079	....	-0.2000	-0.6942	-0.5433
30-0i	0	0.1958	-0.9043	....	-0.3800	-0.3626	-0.6497
30-1i	0	0.1982	-0.8492	....	-0.2224	-0.5677	-0.6211
30-2i	0	0.2081	-0.8232	....	-0.1839	-0.6184	-0.6028
.				....			
.				.			
.				.			
30-17i	0	0.2227	-0.8101	....	-0.1988	-0.6959	-0.5461

3.3.2 Thickness Lookup Matrix

In the thickness lookup matrix, elements are the real and imaginary parts of the simulated reflection coefficient as a function of different thickness values of a specific MUT layer, in the frequency range 3–10 GHz. In order to create this matrix, a particular fluid e.g. ethanol/water 0.76 molar was selected as the MUT layer in the simulation model. The thickness of this layer was defined as a variable and swept in the range 0.2–5 cm with steps of 0.1 cm. This matrix is shown in Tables 3.7 and 3.8 for ethanol/water 0.76 molar, where the elements are the real and imaginary parts of the simulated reflection coefficient, respectively. The same matrices were generated for other fluids listed in Table 3.2.

Table 3.7: The real part of the generated thickness lookup matrix for ethanol/water 0.76 molar.

Thickness(cm)/Freq(GHz)	**3**	**3.5**	**4**	....	**9.5**	**10**
0.2	0	0.6901	0.0751	....	0.3570	-0.1863
0.3	0	0.7117	0.0976	....	0.2328	-0.4171
0.4	0	0.7322	0.0816	....	0.0542	-0.4987
0.5	0	0.7537	0.0536	....	0.0308	-0.3809
0.6	0	0.7701	0.0232	....	0.0551	-0.2437
0.7	0	0.7804	-0.0067	....	0.1575	-0.2562
.				.		
.				.		
.				.		
5	0	0.7467	-0.0164	....	0.1081	-0.3251

Table 3.8: The imaginary part of the generated thickness lookup matrix for ethanol/water 0.76 molar.

Thickness(cm)/Freq(GHz)	**3**	**3.5**	**4**	....	**9.5**	**10**
0.2	0	0.2167	-0.5535	....	-0.4381	-0.5571
0.3	0	0.2221	-0.6299	....	-0.6155	-0.5195
0.4	0	0.2248	-0.6834	....	-0.6217	-0.3446
0.5	0	0.2203	-0.7146	....	-0.4804	-0.2084
0.6	0	0.2083	-0.7298	....	-0.3664	-0.2683
0.7	0	0.1925	-0.7325	....	-0.3983	-0.3762
.				.		
.				.		
.				.		
5	0	0.1669	-0.6739	....	-0.4626	-0.3391

Chapter 4

Experiment

In the first part of this chapter, the experimental setup used for measuring the reflection coefficient is described. In the second part, the corresponding measurement results are presented.

4.1 Experimental Setup

4.1.1 Measurement Setup

The experimental work was carried out at the chemistry laboratory at CMR. The main equipment used in the experimental setup are listed in Table 4.1. Figure 4.1 shows a schematic model of the setup. A photo of the actual experimental setup is shown in Figure 4.2. The network analyzer was connected to the rectangular waveguide sensor by using a coaxial cable. The waveguide sensor was installed at the bottom of a rectangular container (Figure 4.3(a)). A piece of tape was used at the interface to separate the waveguide space from the container space (Figure 4.3(b)). Dimensions of the waveguide and container are listed in Table 4.2.

Table 4.1: The equipment used in the experimental setup.

Equipment	**Model**
Network analyzer	Rohde & Schwarz ZVL13
Rectangular waveguide sensor	R48
Coaxial cable	Rohde & Schwarz ZV-Z191
Calibration kit	Rohde & Schwarz ZV-Z132 CAL KIT
Laptop	Dell Latitude E7240

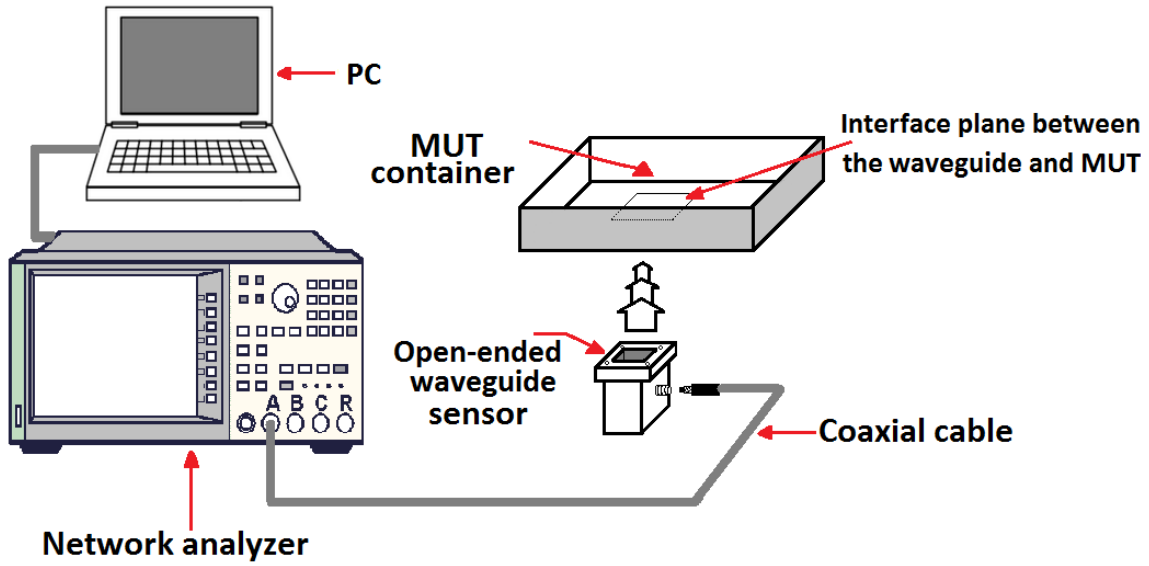

Figure 4.1: A schematic view of the experimental setup.

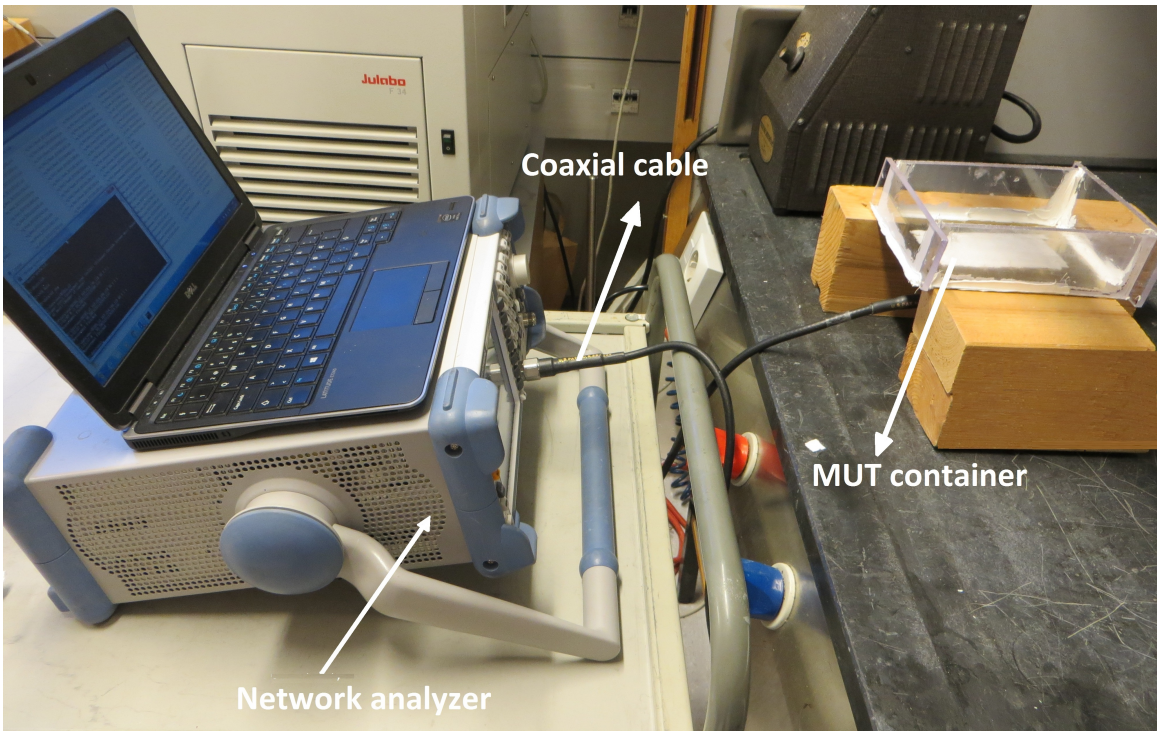

Figure 4.2: A photograph of the experimental setup. The microwaves were transmitted from the network analyzer to the rectangular waveguide sensor.

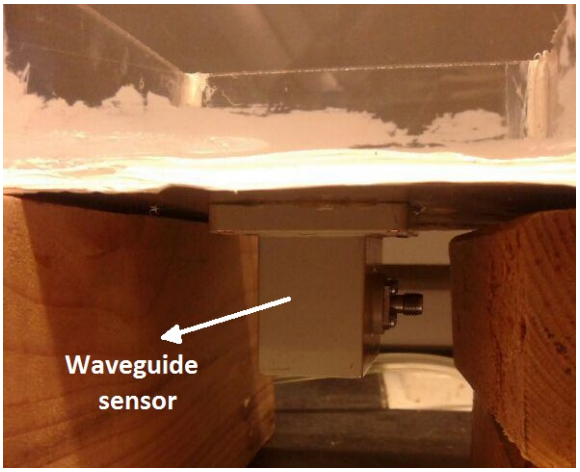

(a)

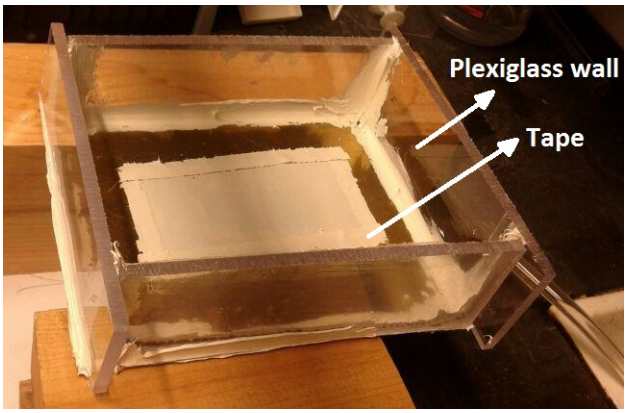

(b)

Figure 4.3: (a) Position of the rectangular waveguide at the bottom of the MUT container. (b) The waveguide opening and the container space were separated by a piece of tape.

Table 4.2: Dimensions of the waveguide sensor and the MUT container.

Tool	**Dimension (length×width×height[cm])**
Waveguide sensor (R48)	4.5 × 4.75 × 2.2
MUT container	15 × 12 × 4

To measure the reflection coefficient for layers thicker than 3 cm, the container was modified. The walls of the original container were removed and new walls with a height of 10 cm were installed (Figure 4.4).

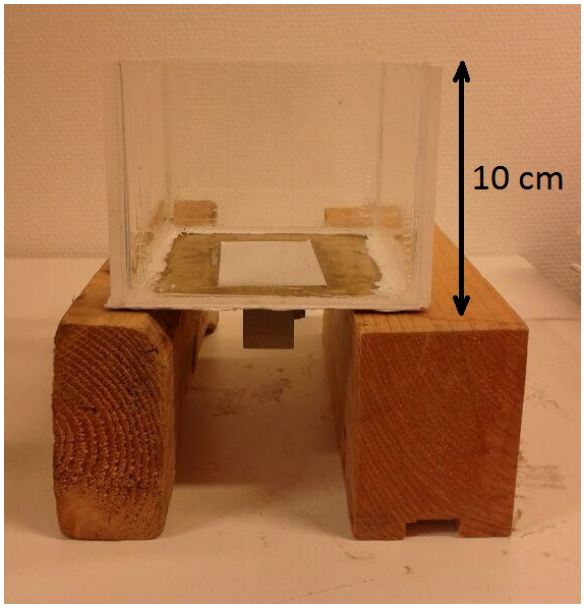

Figure 4.4: A photograph of the container with the higher 10 cm walls.

4.1.2 Fluids Preparation

Several fluids were used in the experimental work of this project for measuring the reflection coefficient listed in Table 4.3. The relevant electrical properties of the fluids were previously presented in Table 3.2. Mixtures of ethanol/water with different concentrations were prepared according to the information in Table 4.4.

Table 4.3: Different test fluids used in the experimental work.
(*: Applied molar fraction of ethanol in the ethanol/water mixture.)

Material under test
Air
Diesel
Ethanol/water $x_e^* = 0.76$
Ethanol/water $x_e = 0.54$
Ethanol/water $x_e = 0.36$
Distilled water

Table 4.4: Ethanol/water mass in the three mixtures.

Molar fraction	Mass of ethanol [g]	Mass of distilled water [g]
$x_e = 0.36$	288	200
$x_e = 0.54$	360	120
$x_e = 0.76$	405	50

The relative permittivity was estimated for three test materials: ethanol/water 0.36 molar, ethanol/water 0.54 molar, and ethanol/water 0.76 molar. The thickness was estimated for four test materials: ethanol/water 0.36 molar, ethanol/water 0.54 molar, ethanol/water 0.76 molar, and diesel. A list of calibration fluids for each MUT is presented in Table 4.5.

Table 4.5: Test materials and calibration fluids used in the relative permittivity and thickness estimation procedure (thickness for all fluids is 3 cm).

MUT	Calibration fluids
Ethanol/water 0.36 molar	Air, Ethanol/water 0.76 molar, Water
Ethanol/water 0.54 molar	Air, Ethanol/water 0.76 molar, Ethanol/water 0.36 molar
Ethanol/water 0.76 molar	Air, Ethanol/water 0.54 molar, Water
Diesel	Air, Ethanol/water 0.76 molar, Water

4.1.3 Reflection Coefficient Measurement

Prior to each experiment, the network analyzer was calibrated at the end of the coaxial cable by means of a calibration kit (ZV-Z132). The frequency was set in the range 0.5–10 GHz with 1001 frequency points. The full calibration mode was selected, and the calibration procedure was repeated for open, short, and match conditions. All measurements were performed at room temperature. In order to measure the reflection coefficient in a thickness range 0–3 cm with steps of 0.5 cm for a specific fluid as the MUT, the procedure was initiated with an empty

container and followed by adding the equivalent of 0.5 cm increments of the fluid to the container, which corresponds to 90 ml. This volume was measured in a glass graduated cylinder. The reflection coefficient measurement was performed for all of the fluids listed in Table 4.3.

To start a new measurement on the next MUT, the container was emptied by sucking the liquid out of the container utilizing a syringe. The remaining fluid was removed by using a paper towel. In the case of water, water/ethanol 0.76 molar, and diesel, the above mentioned procedure was repeated for higher thickness values from 3.5 cm to 5 cm as well.

4.2 Results

4.2.1 Reflection Coefficient Measurement Results

In Figure 4.5, the magnitude and phase values of the measured reflection coefficient (S_{11}^{M}) for the fluids listed in Table 4.3 with a thickness of 3 cm are shown. The magnitude of the reflection coefficient for frequencies less than 3 GHz was found to be approximately 1. This means that at these frequencies, the microwaves were totally reflected at the end of the coaxial cable and no signal propagated in the waveguide. That is because, the waveguide cutoff frequency for R48 is approximately 3 GHz.

Figures 4.6, 4.7,and 4.8 show the real and imaginary parts of the reflection coefficient in a frequency range 0.5–10 GHz for different thickness values of ethanol/water 0.36 molar, ethanol/water 0.54 molar, and ethanol/water 0.76 molar, respectively.

According to the figures, it was found that the reflection coefficient did not change significantly by changing the thickness of the MUT layer. This was not the case for all of the fluids in Table 4.3. For example for diesel, changing the thickness changed the reflection coefficient curve clearly. Figure 4.9 depicts the real and imaginary parts of the reflection coefficient in a frequency range 0.5–10 GHz for different thickness values of diesel.

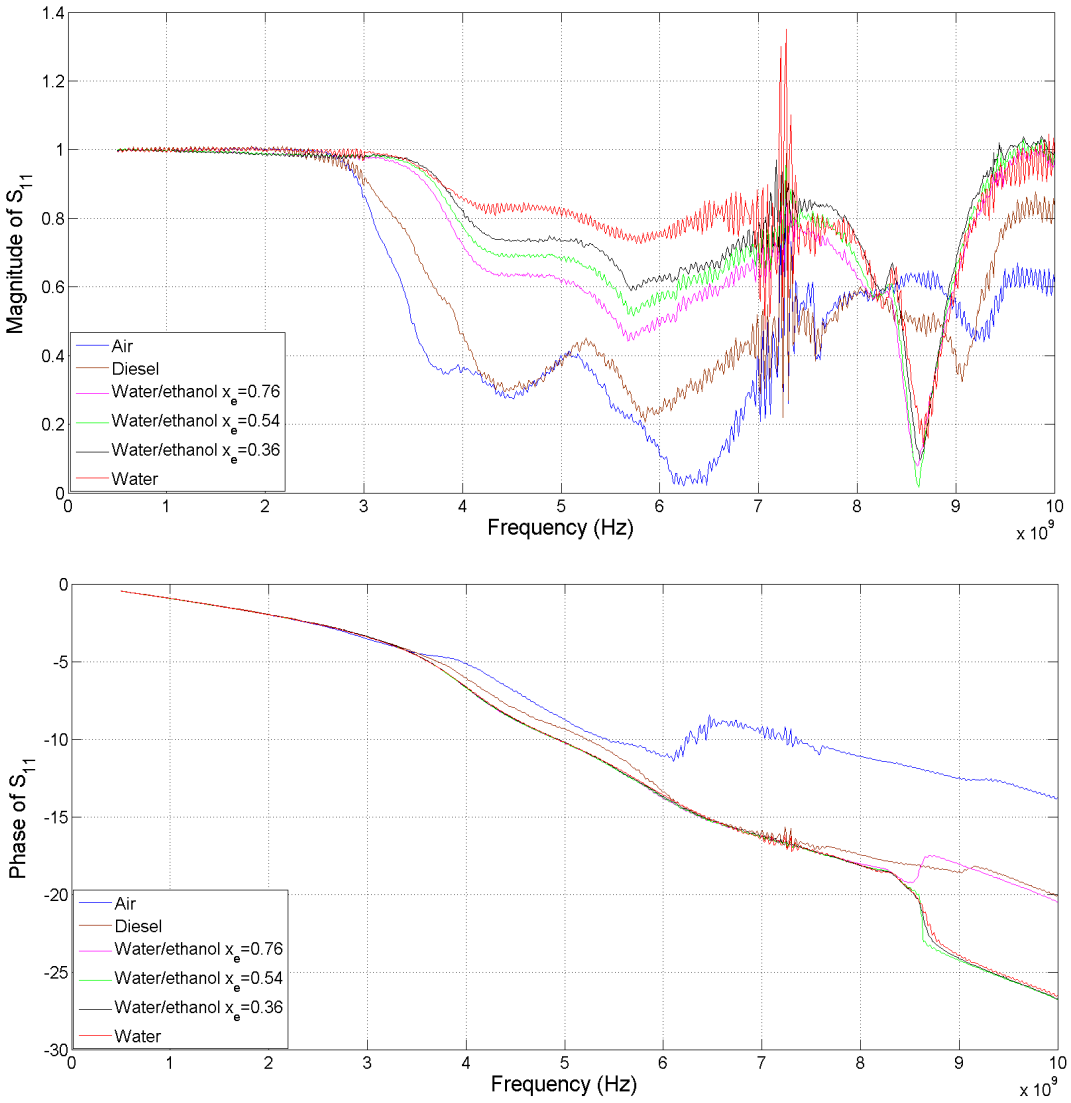

Figure 4.5: The magnitude and phase values of the measured S_{11} parameter for six fluids with a thickness of 3 cm in the frequency range 0.5–10 GHz. The phase increases as a function of frequency which is not physically correct, but is due to noise affecting the phase wrapping in MATLAB.

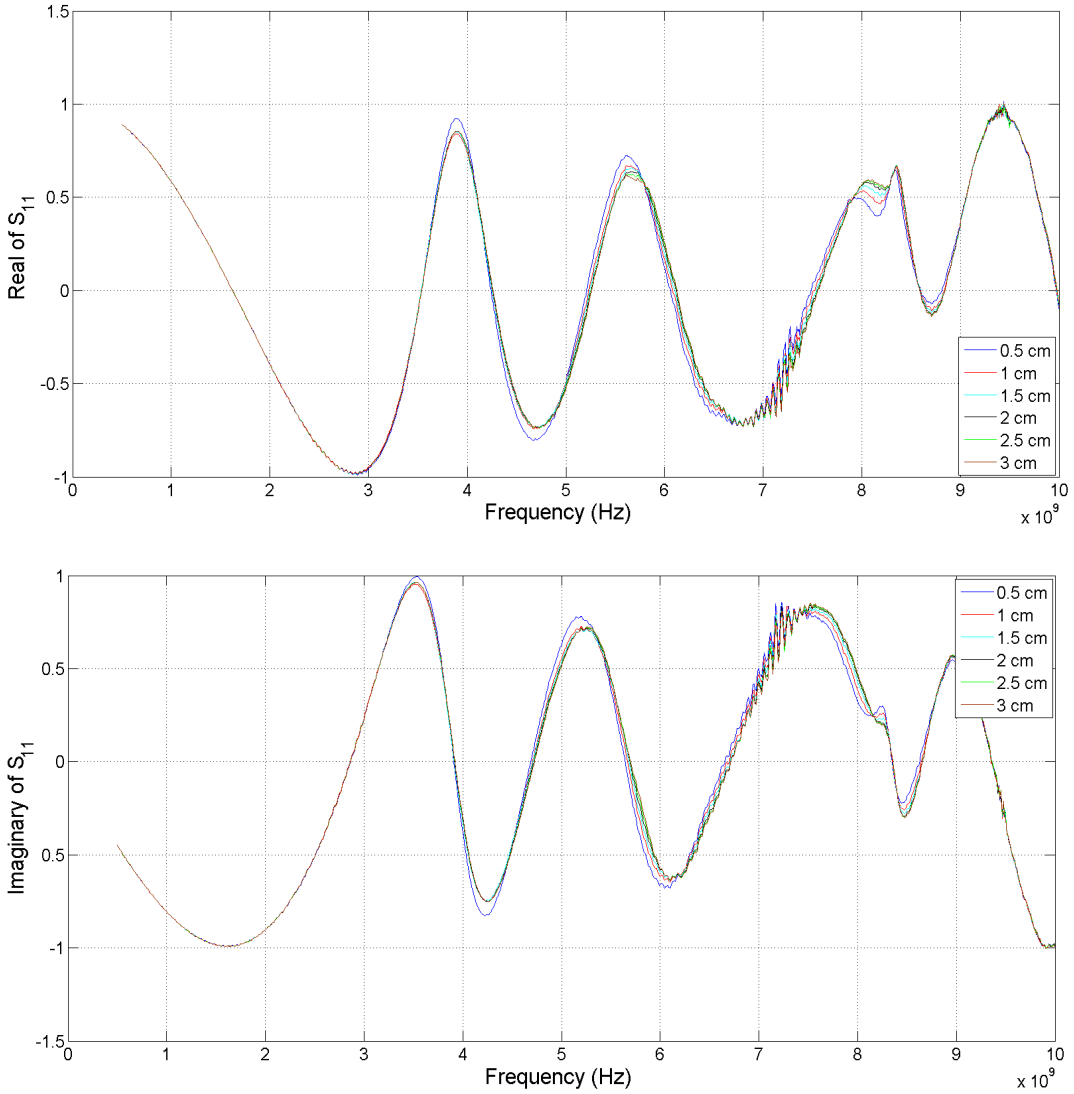

Figure 4.6: The real and imaginary parts of the measured S_{11} parameter for ethanol/water 0.36 molar in the thickness range 0.5–3 cm and frequency range 0.5–10 GHz.

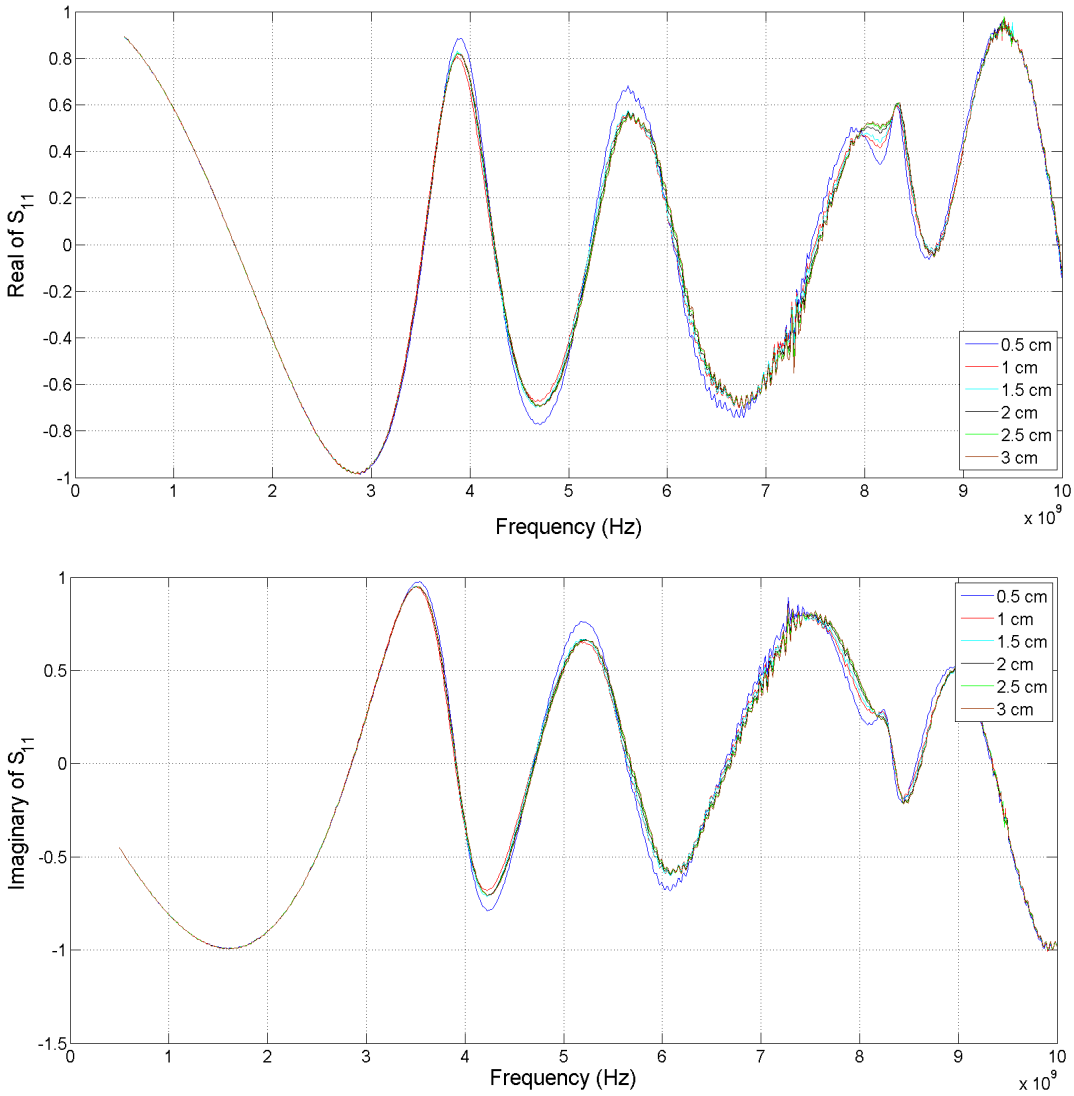

Figure 4.7: The real and imaginary parts of the measured S_{11} parameter for ethanol/water 0.54 molar in the thickness range 0.5–3 cm and frequency range 0.5–10 GHz.

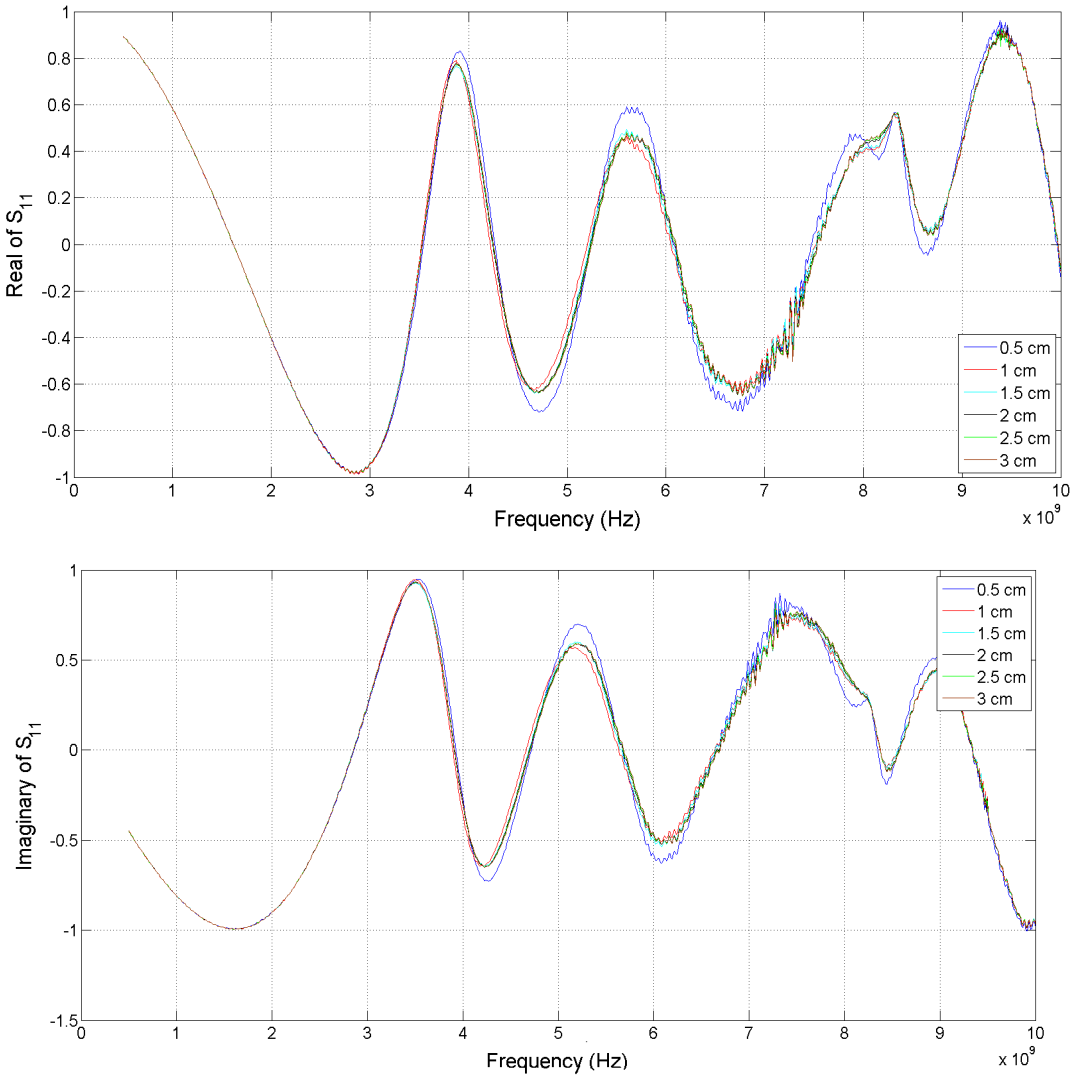

Figure 4.8: The real and imaginary parts of the measured S_{11} parameter for ethanol/water 0.76 molar in the thickness range 0.5–3 cm and frequency range 0.5–10 GHz.

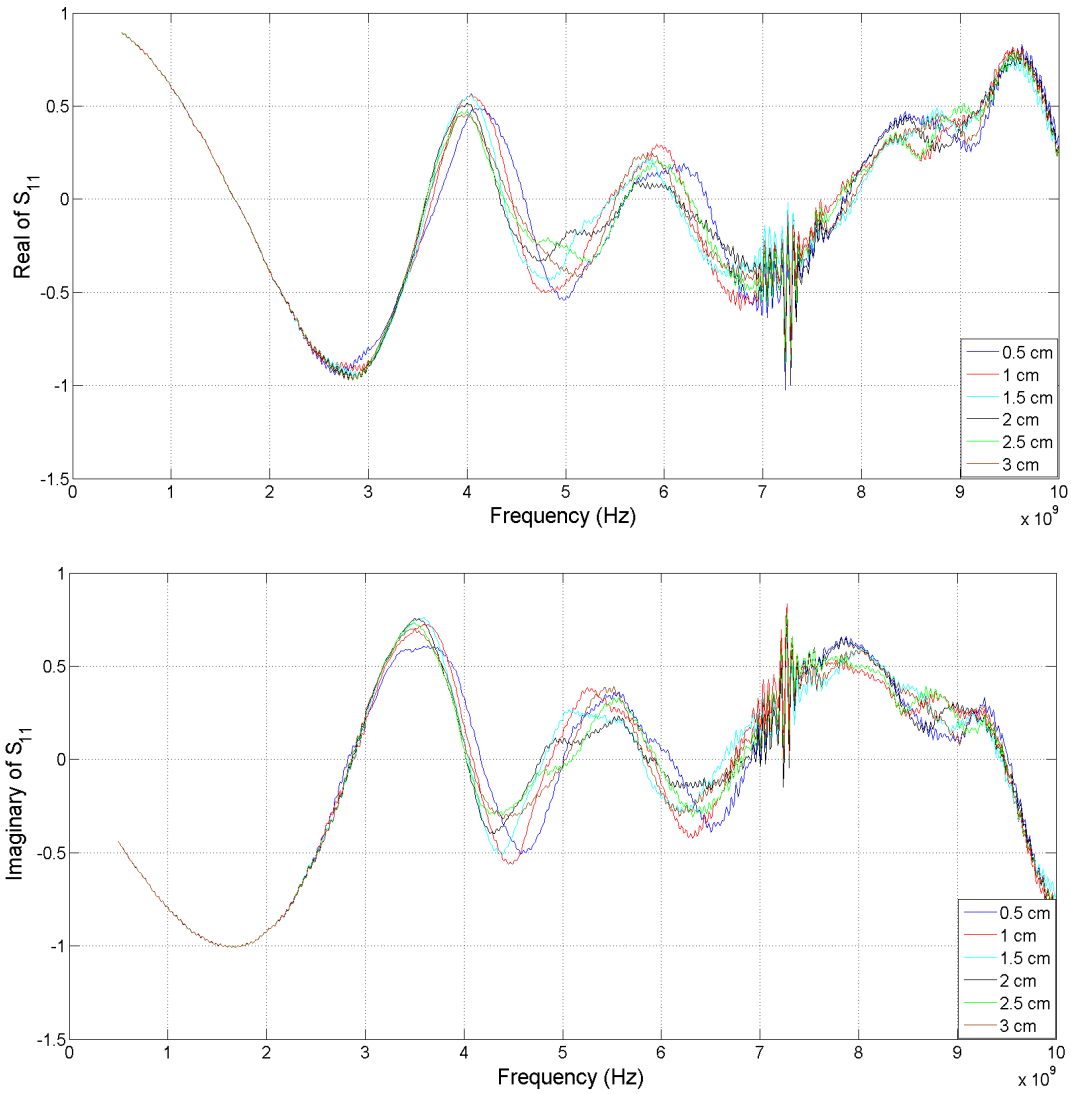

Figure 4.9: The real and imaginary parts of the measured S_{11} parameter for diesel in the thickness range 0.5–3 cm and frequency range 0.5–10 GHz.

4.2.2 Measurement Uncertainty

When a set of several repeated readings (N= number of readings) has been taken, the mean, $\bar{x}$, and the standard deviation, s, can be calculated for the set. From these, the estimated standard uncertainty of the mean value, u_{avg}, is calculated:

$$u_{avg} = \frac{s}{\sqrt{N}} \ . \tag{4.1}$$

Uncertainty can be calculated for a single new measurement (sample) as well. Assuming a 95% confidence interval, the uncertainty of the new measurement is obtained from:

$$u = 2s \ . \tag{4.2}$$

To calculate the standard uncertainty, the reflection coefficient was measured for air and 3 different thicknesses (d=1, 2, and 3 cm) of water in the frequency range 0.5–10 GHz. The measurements were repeated 6 times (N=6), following each other, for each fluid and thickness. Before each measurement, the network analyzer was calibrated at the end of the coaxial cable. By doing so, the contribution of the network analyzer, the coaxial cable, and the calibration kit in calculating the standard uncertainty were taken into account. However, some other sources of uncertainty such as the uncertainty of the operator in preparing the fluids or the uncertainty caused by environmental effects like temperature variations were not included. Figure 4.10 shows the real and imaginary parts of the standard deviation of the measured reflection coefficient in the case of air and 3 different thicknesses of water in the frequency range 0.5–10 GHz. Table 4.6 represents the average standard uncertainty of the measured reflection coefficient in the whole frequency range for each case.

Table 4.6: Standard uncertainty of the measured reflection coefficient.

MUT layer	$\mathbf{u_{avg}}$	**u**
Air	0.0038 + 0.0039i	0.0187 + 0.0190i
Water:		
1 cm	0.0041 + 0.0040i	0.0199 + 0.0196i
2 cm	0.0020 + 0.0021i	0.0100 + 0.0102i
3 cm	0.0025 + 0.0024i	0.0120 + 0.0119i

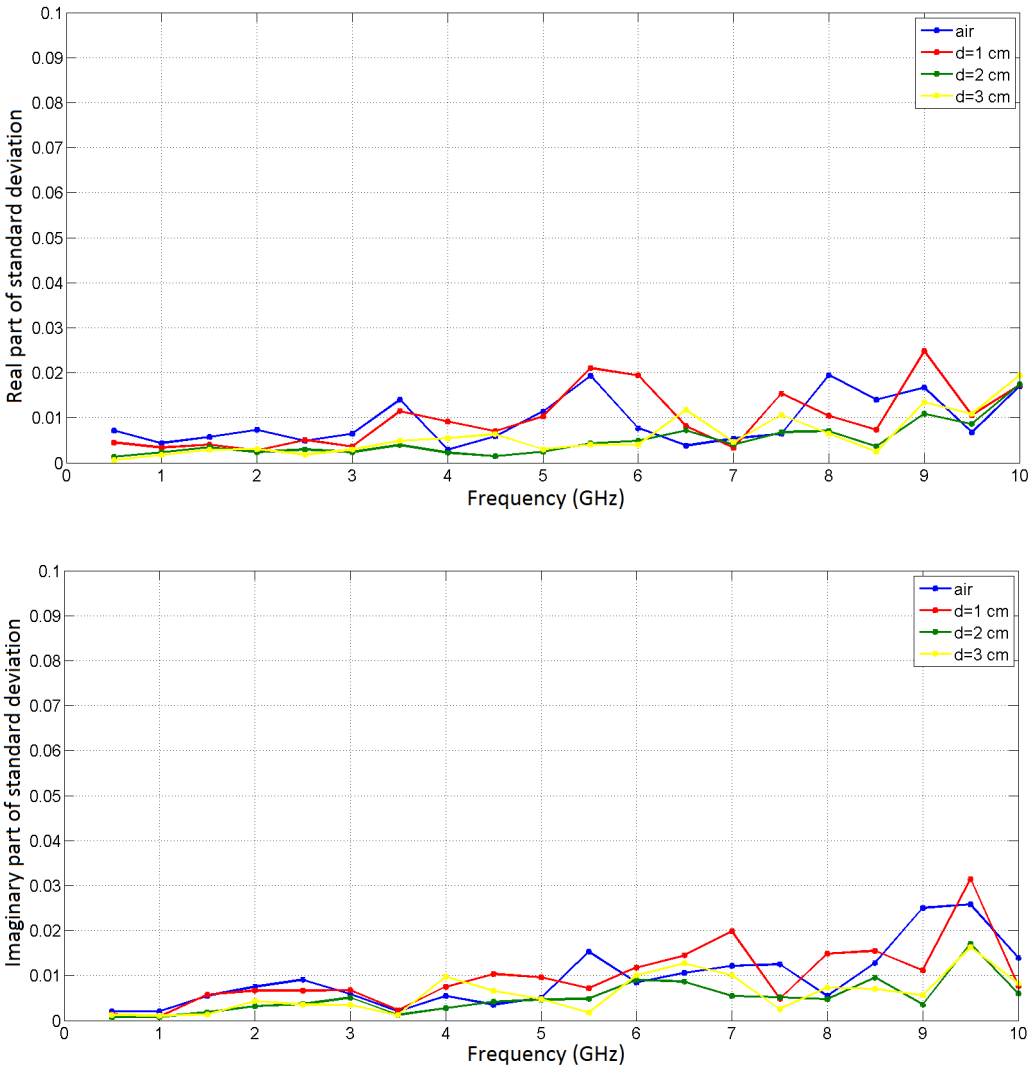

Figure 4.10: The real and imaginary parts of the standard deviation of the measured reflection coefficient in the case of air and 3 different thicknesses of water in the frequency range 0.5–10 GHz.

This page is intentionally left blank

Chapter 5

Result Analysis and Discussion

In this chapter, the results of the relative permittivity estimation for three test fluids: mixtures of ethanol/water 0.36 molar, 0.54 molar, and 0.76 molar; and the results of the thickness estimation for four test fluids: mixtures of ethanol/water 0.36 molar, 0.54 molar, 0.76 molar, and diesel are presented and compared with the corresponding actual values.

5.1 Comparison of the Simulation and Measurement Results

Figures 5.1, 5.2, and 5.3 show the magnitude and phase of the simulated, measured (S_{11}^{M}), and transformed (S_{11}^{R}) reflection coefficients for ethanol/water 0.54 molar, ethanol/water 0.76 molar, and diesel with a thickness of 3 cm. In the case of ethanol/water 0.36 molar, the figure was previously presented in Section 3.2.

Regarding the figures, there was a deviation between the simulated and measured reflection coefficients over the whole frequency range. As discussed earlier (in Section 3.2), this deviation came from a phase lag between the simulation and measurement results. Therefore, the measurement results were calibrated and transformed through the bilinear transformation which resulted in the transformed reflection coefficients. It was found that in the range 4–6 GHz, the mean value of the calibration error (Eq. 3.3) was 6.44%, 6.40%, and 22.79% for ethanol/water 0.54 molar, 0.76 molar, and diesel, respectively. Therefore, it was concluded that the transformed reflection coefficient followed the simulated reflection coefficient fairly good at this frequency range. However, for the frequencies higher than 6 GHz, the mean value of the calibration error was more than 50% for the three fluids (more explanation in Section 5.2).

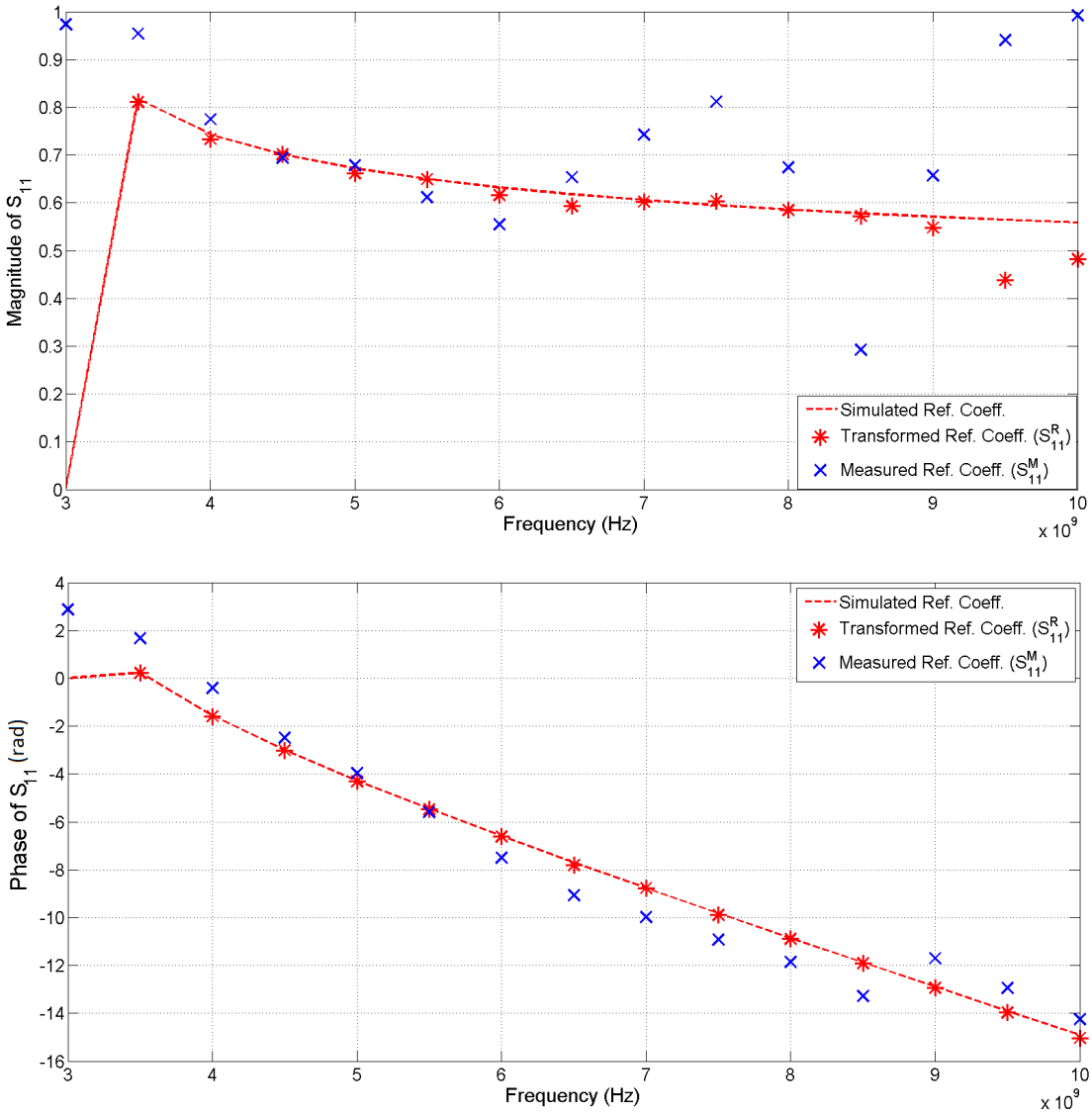

Figure 5.1: The magnitude and phase of the transformed, simulated, and measured reflection coefficients for ethanol/water 0.54 molar ($x_e = 0.54$) with a thickness of 3 cm.

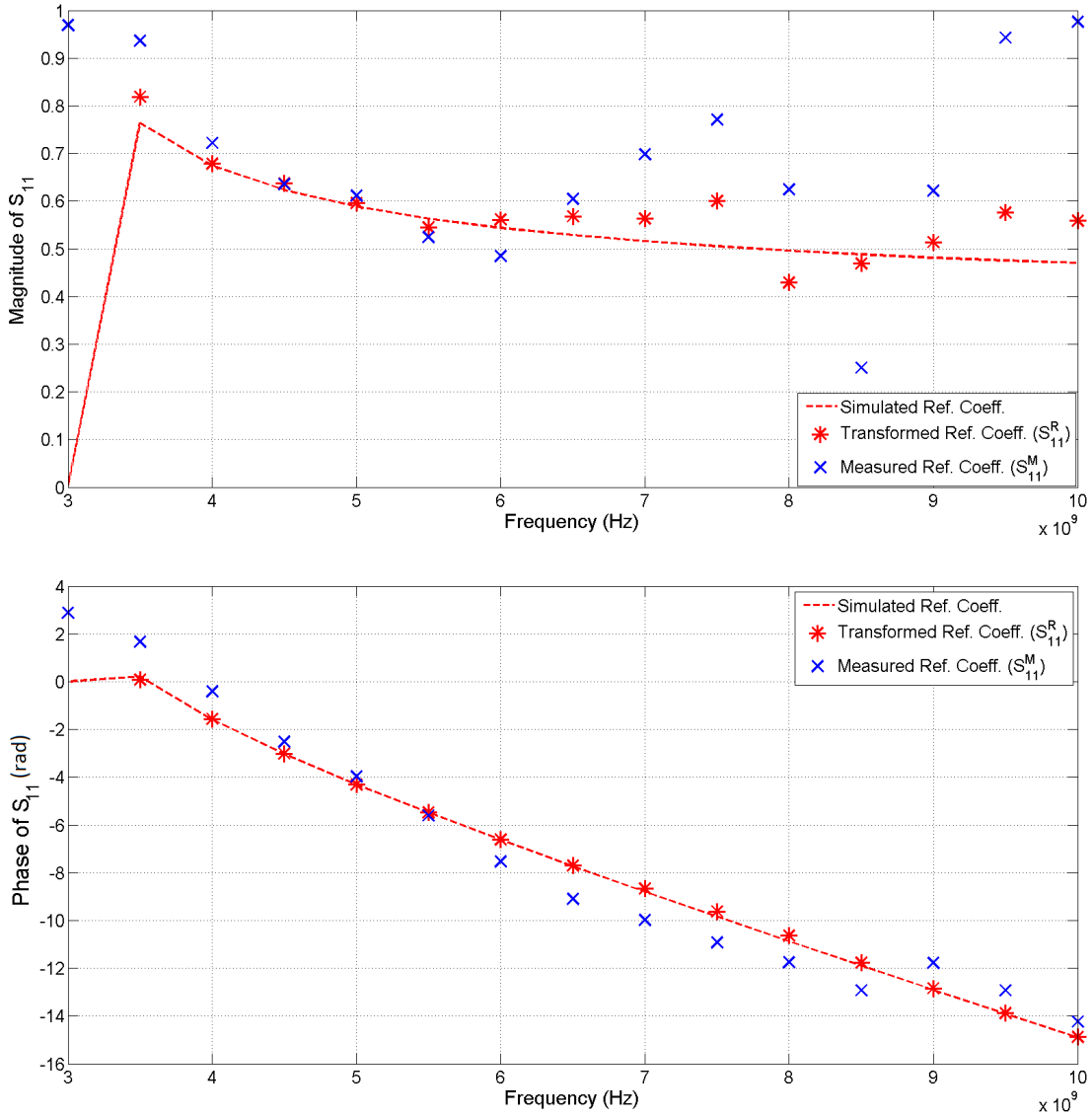

Figure 5.2: The magnitude and phase of the transformed, simulated, and measured reflection coefficients for ethanol/water 0.76 molar ($x_e = 0.76$) with a thickness of 3 cm.

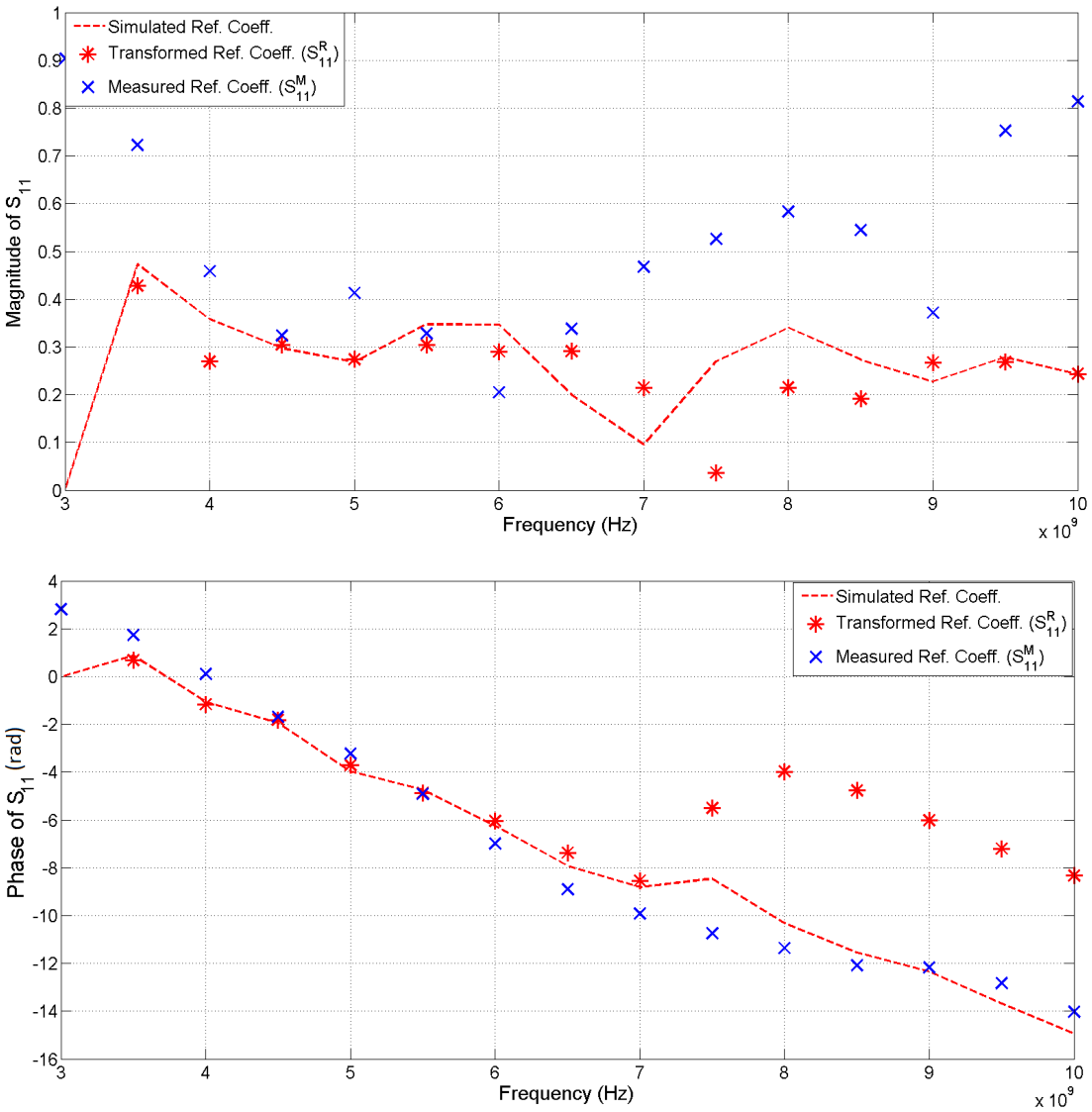

Figure 5.3: The magnitude and phase of the transformed, simulated, and measured reflection coefficients for diesel with a thickness of 3 cm.

5.2 Relative Permittivity Estimation

The relative permittivity of the three test fluids, ethanol/water 0.36 molar, 0.54 molar, and 0.76 molar with a thickness of 3 cm were estimated using the permittivity lookup matrix. The results of the permittivity estimation for the frequency range 4–10 GHz are presented in Tables 5.1, 5.2, and 5.3. In these tables, the second column represents the calculated relative permittivity from the Cole-Cole equation (see Eq. 2.12 and Table 3.2) as the actual value, the third column shows what was expected from the estimation (based on the resolution in the lookup matrix), and the last column lists the result of the relative permittivity estimation using the permittivity lookup matrix.

The complex value in the parenthesis shows the uncertainty of the estimation. In order to calculate the uncertainty, it was assumed that the uncertainty of the transformed reflection coefficient was equal to the uncertainty of the measured reflection coefficient (see Table 4.6). Then, using the lookup matrix, the relative permittivity was estimated for two cases: transformed reflection coefficient plus uncertainty and transformed reflection coefficient minus uncertainty. The worse case is reported as the uncertainty in the tables.

Table 5.1: Results of the permittivity estimation for ethanol/water 0.36 molar.

Freq (GHz)	**Calculated ε_r^* (Cole-Cole equation)**	**Expected ε_r^***	**Estimated ε_r^***
4	22.16 – 16.67i	22 – 17i	27 – 17i (±(5-i))
4.5	20.37 – 15.97i	20 – 16i	18 – 13i (±(4-i))
5	18.91 – 15.22i	19 – 15i	20 – 12i (±(3-i))
5.5	17.71 – 14.46i	18 – 14i	21 – 17i (±(1-i))
6	16.72 – 13.73i	17 – 14i	18 – 13i (±(3-i))
- -	- - - - - - - -	- - - - -	- - - - - - - -
6.5	15.91 – 13.04i	16 – 13i	12 – 4i
7	15.22 – 12.39i	15 – 12i	2 – 10i
7.5	14.65 – 11.79i	15 – 12i	29 – 0i
8	14.16 – 11.23i	14 – 11i	24 – 0i
8.5	13.75 – 10.71i	14 – 11i	12 – 0i
9	13.39 – 10.23i	13 – 10i	11 – 12i
9.5	13.08 – 9.78i	13 – 10i	7 – 5i
10	12.81 – 9.37i	13 – 9i	6 – 4i

Table 5.2: Results of the permittivity estimation for ethanol/water 0.54 molar.

Freq (GHz)	**Calculated ε_r^* (Cole-Cole equation)**	**Expected ε_r^***	**Estimated ε_r^***
4	13.73 – 11.32i	14 – 11i	12 – 11i (±(1-3i))
4.5	12.74 – 10.50i	13 – 11i	12 – 11i (±(2-i))
5	11.98 – 9.76i	12 – 10i	10 – 10i (±(1-i))
5.5	11.39 – 9.08i	11 – 9i	11 – 9i (±(1-i))
6	10.91 – 8.48i	11 – 8i	9 – 8i (±(2-i))
- -	- - - - - - - -	- - - - -	- - - - - - - -
6.5	10.53 – 7.95i	11 – 8i	6 – 8i
7	10.22 – 7.47i	10 – 7i	10 – 7i
7.5	9.97 – 7.04i	10 – 7i	8 – 9i
8	9.75 – 6.65i	10 – 7i	9 – 8i
8.5	9.57 – 6.30i	10 – 6i	9 – 7i
9	9.42 – 5.99i	9 – 6i	8 – 6i
9.5	9.29 – 5.70i	9 – 6i	5 – 3i
10	9.18 – 5.43i	9 – 5i	5 – 5i

Table 5.3: Results of the permittivity estimation for ethanol/water 0.76 molar.

Freq (GHz)	**Calculated ε_r^* (Cole-Cole equation)**	**Expected ε_r^***	**Estimated ε_r^***
4	7.96 – 7.18i	8 – 7i	9 – 6i (±(1-2i))
4.5	7.50 – 6.52i	8 – 7i	8 – 7i (±(2-i))
5	7.17 – 5.95i	7 – 6i	7 – 6i (±(1-i))
5.5	6.91 – 5.47i	7 – 5i	7 – 5i (±(1-i))
6	6.71 – 5.06i	7 – 5i	7 – 5i (±(1-i))
- -	- - - - - - -	- - - -	- - - - - - - -
6.5	6.55 – 4.70i	7 – 5i	8 – 5i
7	6.43 – 4.39i	6 – 4i	9 – 3i
7.5	6.32 – 4.12i	6 – 4i	13 – 2i
8	6.24 – 3.87i	6 – 4i	7 – i
8.5	6.17 – 3.66i	6 – 4i	6 – 2i
9	6.11 – 3.46i	6 – 3i	8 – 3i
9.5	6.06 – 3.29i	6 – 3i	10 – 6i
10	6.01 – 3.13i	6 – 3i	9 – 5i

Figures 5.4 and 5.5 show the expected and estimated dielectric constants and loss factors for the three mixtures in the frequency range 4–6 GHz. In the case of estimated values, the uncertainty bars are shown as well. The error of the relative permittivity estimation procedure was calculated from:

$$Estimation\ Error = \sqrt{(\frac{\varepsilon^{'}_{r.exp} - \varepsilon^{'}_{r.est}}{\varepsilon^{'}_{r.exp}})^2 + (\frac{\varepsilon^{''}_{r.exp} - \varepsilon^{''}_{r.est}}{\varepsilon^{''}_{r.exp}})^2} \tag{5.1}$$

where $\varepsilon^{'}_{r.exp}$ and $\varepsilon^{'}_{r.est}$ are the relative dielectric constants, and $\varepsilon^{''}_{r.exp}$ and $\varepsilon^{''}_{r.est}$ are the loss factors of the expected and estimated relative permittivity, respectively. The mean value of the estimation error for ethanol/water 0.36, 0.54, and 0.76 molar was calculated to be 20.21%, 11.37%, and 3.80%, respectively. Assuming that an estimation error of up to 25% is acceptable, it was found that there was a good agreement between the expected and estimated values in the frequency range 4–6 GHz. As it is clear from the results, the lower permittivity fluid resulted in a better permittivity estimation.

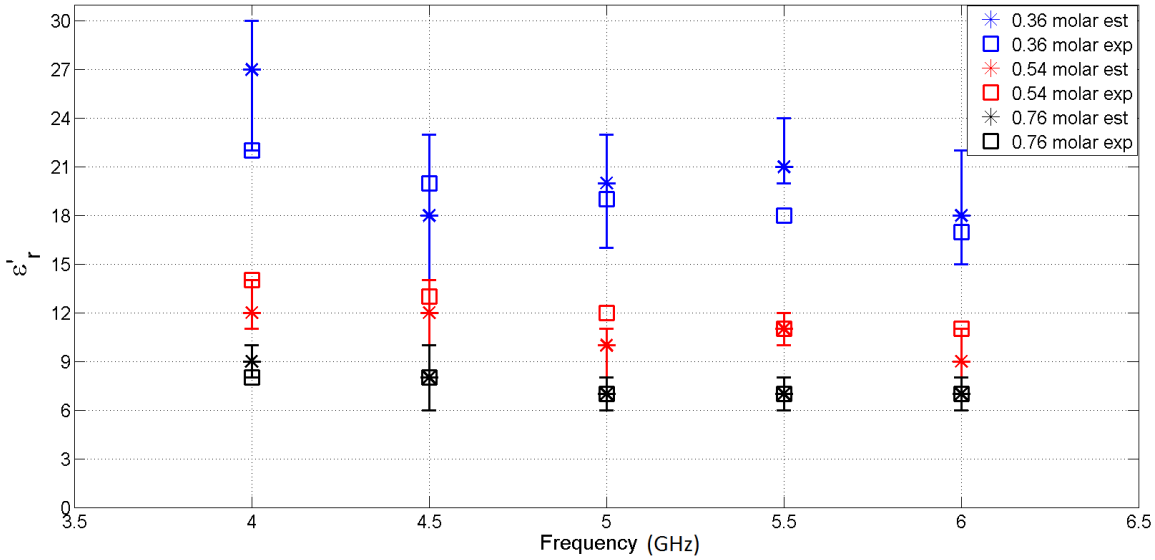

Figure 5.4: The estimated and expected dielectric constants ($\varepsilon^{'}_{r.est}$ and $\varepsilon^{'}_{r.exp}$, respectively) for the mixtures of ethanol/water in the frequency range 4–6 GHz. The uncertainty bars around the estimated values are also depicted.

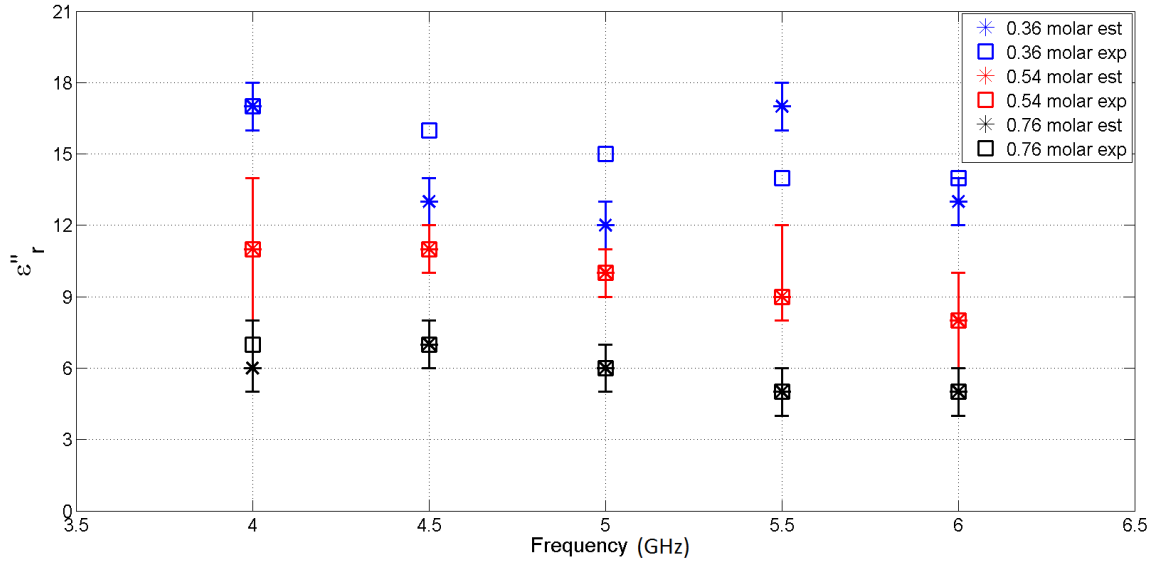

Figure 5.5: The estimated and expected loss factors ($\varepsilon''_{r.est}$ and $\varepsilon''_{r.exp}$, respectively) for the three mixtures of ethanol/water in the frequency range 4–6 GHz. The uncertainty bars around the estimated values are also depicted.

As it was shown in Tables 5.1, 5.2, and 5.3, for frequencies higher than 6 GHz, there was a significant error in the relative permittivity estimation.

It was observed as well from Figures 3.8, 5.1, and 5.2 that in the frequency range 6–10 GHz, the transformed reflection coefficient did not follow the simulated reflection coefficient in an acceptable manner. One reason is that, since the simulation model was perfectly symmetrical, some of the higher order modes could not be excited to propagate in the simulated waveguide. However, the experimental setup was not symmetrical, and therefore some additional higher order modes presented and interfered with the TE10 mode. As calculated in Section 3.1.3, the first cutoff frequency of the waveguide was 3.16 GHz. The second cutoff frequency corresponding to the TE_{20} is calculated from Eq. 2.32 to be $f_{20} = 6.32$ GHz. Thus, for frequencies higher than 6.32 GHz, the second order mode also existed in the experimental waveguide and interfered with the dominant mode. This caused some errors in the relative permittivity estimation. In addition, it is expected that unintentional movements in the coaxial cable introduced some noise in the reflection coefficient measurement, which increased the error of the estimation at high frequencies.

5.3 Thickness Estimation

The thickness of the MUT layer was estimated for the same three fluids as well as diesel. Figures 5.6, 5.7, and 5.8 show the thickness estimation results for ethanol/water 0.36, 0.54, and 0.76 molar, respectively. In order to calculate the uncertainty, it was assumed that the uncertainty of the transformed reflection coefficient was equal to the uncertainty of the measured reflection coefficient (see Table 4.6). Then, using the lookup matrix, the thickness was estimated for two cases: transformed reflection coefficient plus uncertainty and transformed reflection coefficient minus uncertainty. The result is shown as a bar around each of the estimated thickness values in the figures.

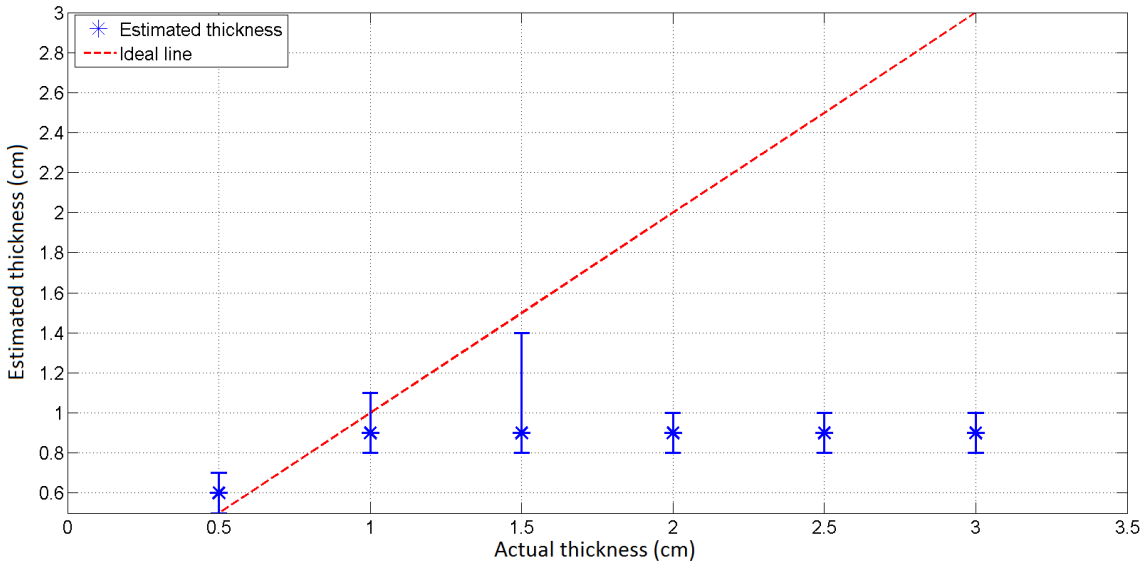

Figure 5.6: Result of the thickness estimation for ethanol/water 0.36 molar in the thickness range 0.5–3 cm.

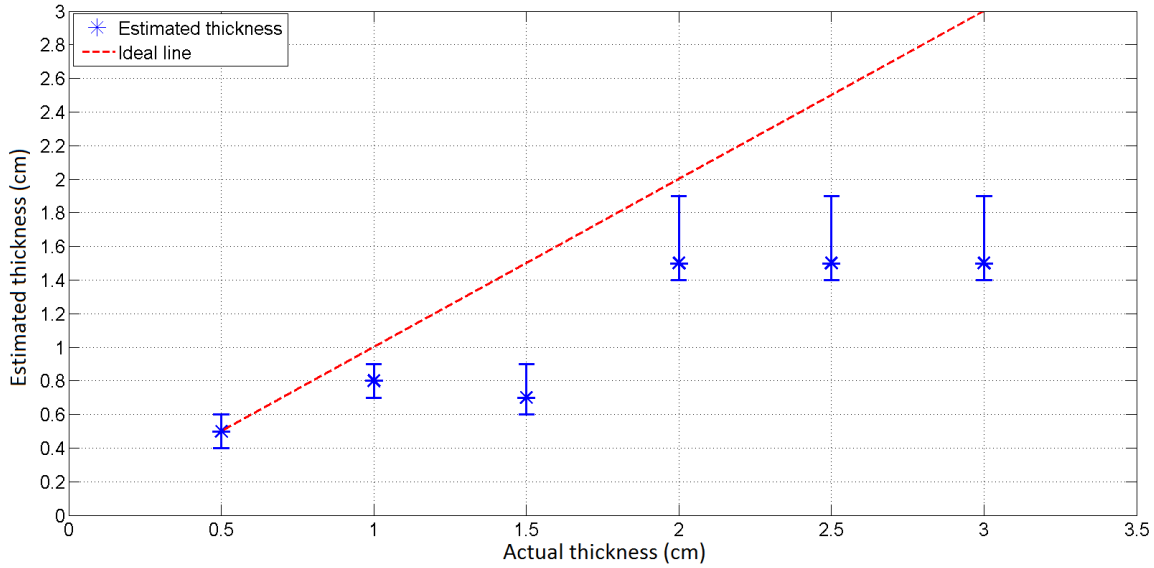

Figure 5.7: Result of the thickness estimation for ethanol/water 0.54 molar in the thickness range 0.5–3 cm.

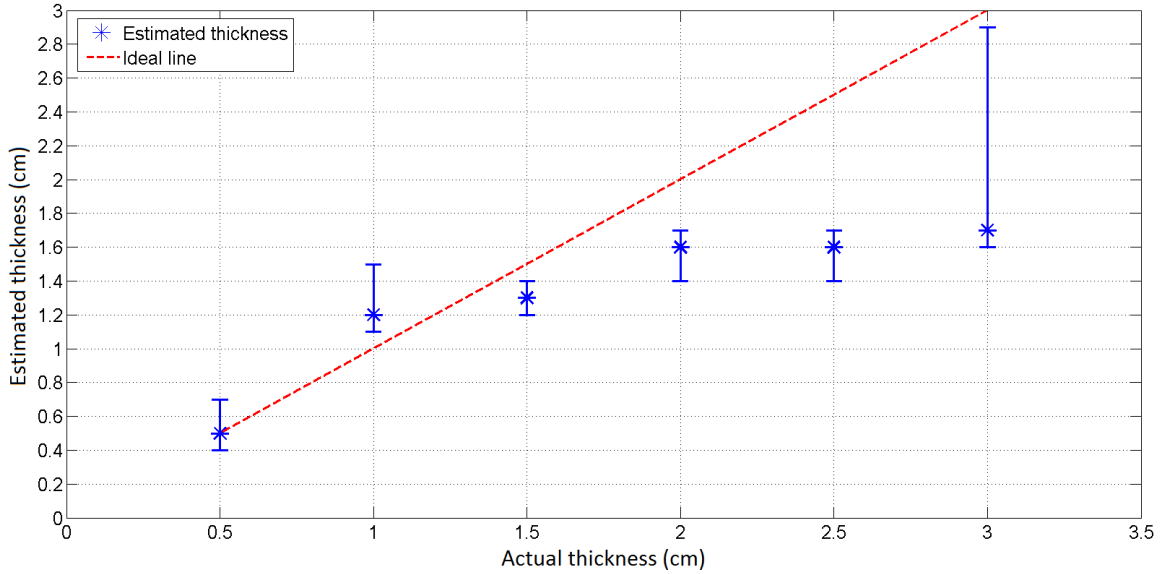

Figure 5.8: Result of the thickness estimation for ethanol/water 0.76 molar in the thickness range 0.5–3 cm.

The error of the thickness estimation procedure was defined as:

$$Estimation\ Error = \frac{d_{act} - d_{est}}{d_{act}} \tag{5.2}$$

where d_{act} is the actual thickness and d_{est} is the estimated thickness. The mean value of the estimation error was calculated to be:

- 15.00% and 20.00% for ethanol/water 0.36 and 0.54 molar, respectively, with a thickness layer up to 1 cm,
- 13.25% for ethanol/water 0.76 molar, with a thickness layer up to 2 cm.

The estimation error was more than 50% in the case of thicker layers, and therefore it was not included in the above mean values.

Assuming that an estimation error of up to 25% is acceptable, it was found that the thickness estimation procedure provided reasonable results in the two following cases:

- Thin layer up to 1 cm for ethanol/water 0.36 and 0.54 molar.
- Thin layer up to 2 cm for ethanol/water 0.76 molar.

In case of each actual thickness, the total deviation between the transformed reflection coefficient and the corresponding elements of the thickness lookup matrix was calculated. Figures 5.9, 5.10, and 5.11 show the total deviation versus each individual actual thickness value of the three mixtures of ethanol/water. For example as shown in Figure 5.9, for actual thickness of 0.5 cm, it was found that the total deviation was minimum for the thickness value of 0.6 cm in the lookup matrix. Therefore, the estimated thickness was assumed to be 0.6 cm. in the case of actual thickness of 1 cm, the minimum occurred at 0.9 which represented the estimated thickness. However, for actual thicknesses higher than 1 cm, there was no absolute minimum in the corresponding curves. The same behavior was also observed in the case of Figures 5.10, and 5.11. Therefore, it was concluded that for the three mixtures of ethanol/water with layers thicker than 1 cm, the estimated thickness results were neither acceptable nor robust.

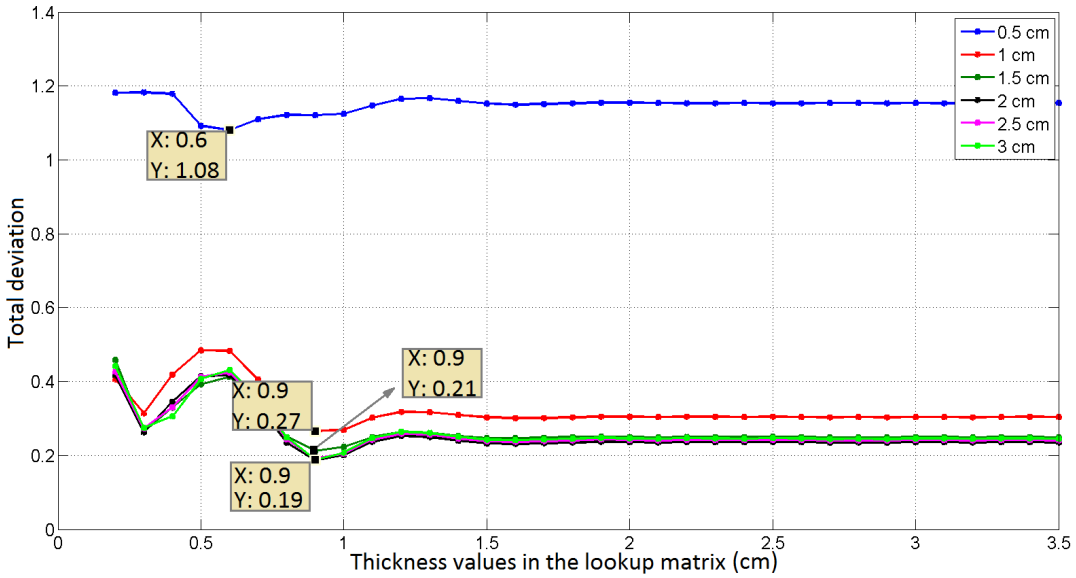

Figure 5.9: Total deviation between the transformed reflection coefficient and the corresponding elements of the thickness lookup matrix in estimating the thickness of ethanol/water 0.36 molar. The amount of minimum total deviation is highlighted for each actual thickness value.

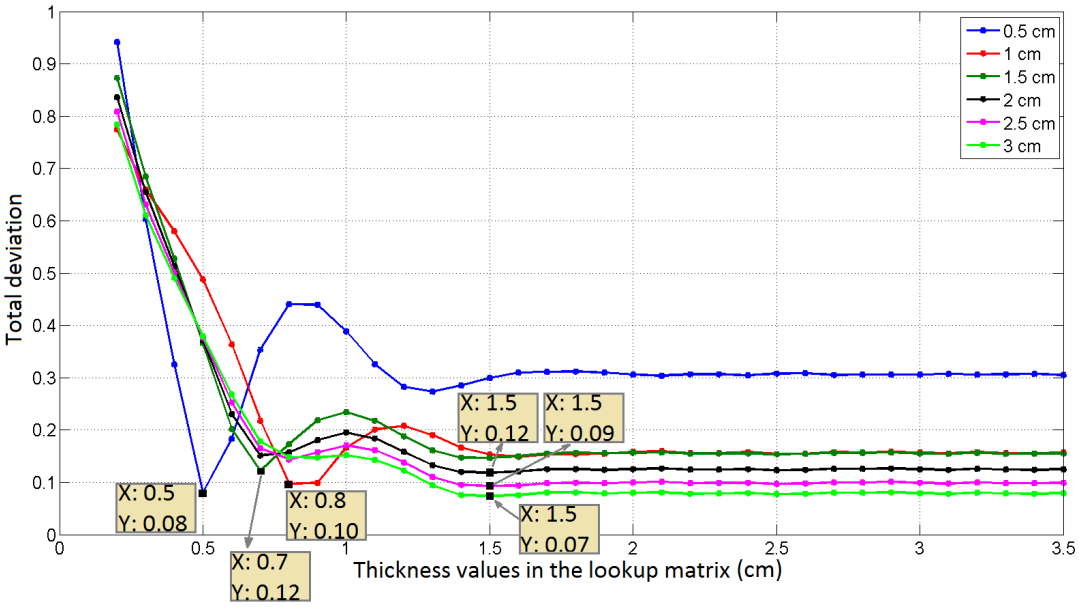

Figure 5.10: Total deviation between the transformed reflection coefficient and the corresponding elements of the thickness lookup matrix in estimating the thickness of ethanol/water 0.54 molar. The amount of minimum total deviation is highlighted for each actual thickness value.

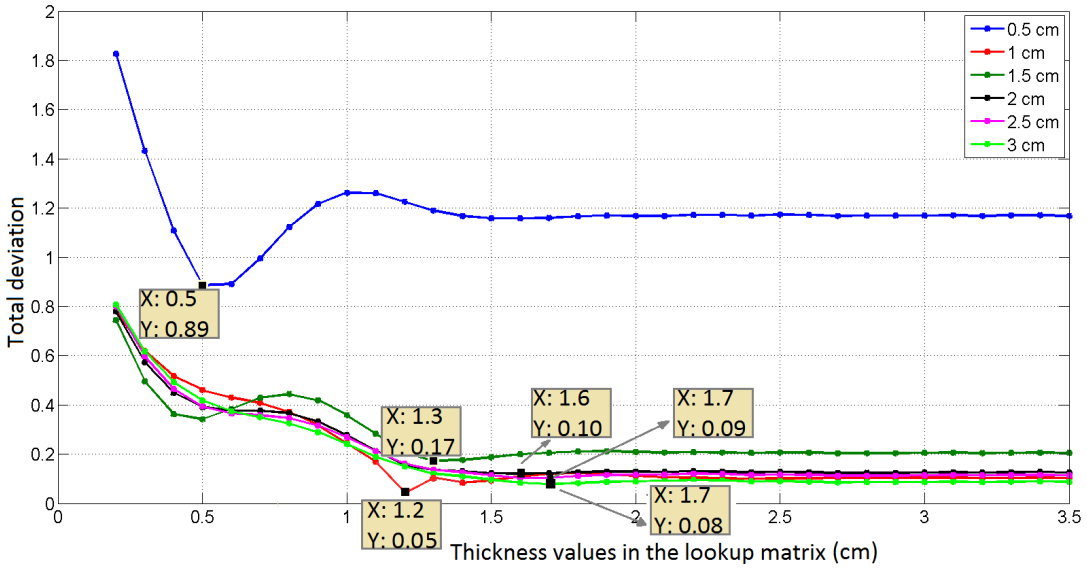

Figure 5.11: Total deviation between the transformed reflection coefficient and the corresponding elements of the thickness lookup matrix in estimating the thickness of ethanol/water 0.76 molar. The amount of minimum total deviation is highlighted for each actual thickness value.

The reason for the above behavior of the ethanol/water mixtures could be explained from the measurement results: As shown in Figures 4.6, 4.7, and 4.8 before, the measured reflection coefficient was almost independent of the thickness variations, particularly for thickness values higher than 1 cm. This could be due to:

- A large reflection from the interface of the waveguide and MUT layer (main reflection), compared with the secondary reflections through the layer which were affected by the MUT thickness (see Figure 1.1). This means that the main reflection was so large that the secondary reflections were negligible, and therefore the measured reflection coefficient was not affected by the MUT thickness variations. This could also be explained from the simulation results. The magnitude of the simulated reflection coefficients for the ethanol/water mixtures with a thickness of 3 cm is shown in Figure 5.12. According to the figure, for the three mixtures, the magnitude of the S_{11} parameter decreased smoothly from a high value around 0.9, without oscillation. However, for a thin layer for instance 1 cm, some weak oscillations appeared, as shown in Figure 5.13. The oscillations, in fact, represented the secondary reflections. Therefore, in the case of three mixtures, the thickness estimation procedure gave an acceptable result only for layers up to 1 cm.

- Large attenuation of the microwaves through ethanol/water mixtures. Figure 5.14 shows the attenuation constant, α, as a function of frequency for the three mixtures. The large α value caused that the secondary reflections were strongly attenuated compared with the the main reflection, and therefore the reflection coefficient was almost not affected by the thickness variations.

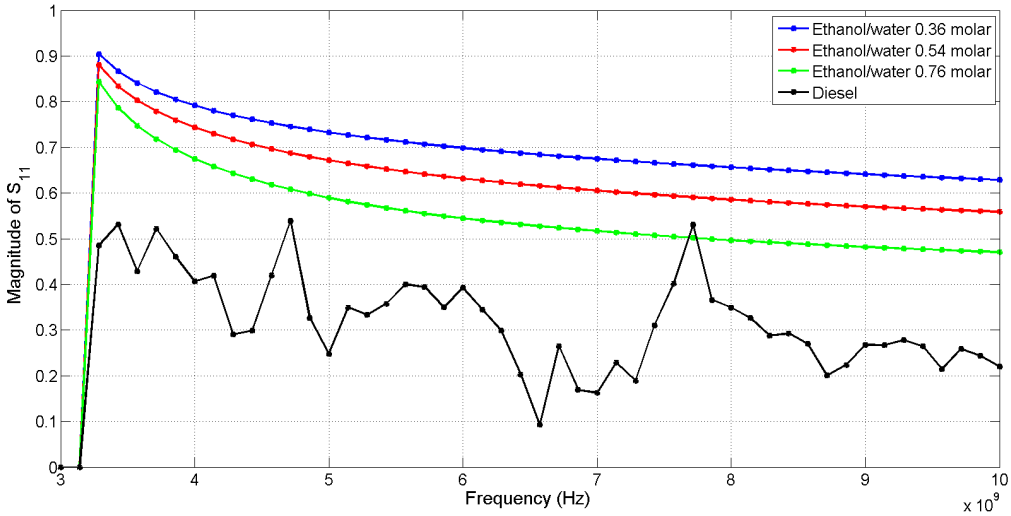

Figure 5.12: The magnitude of the simulated reflection coefficient for the three mixtures of ethanol/water and diesel with a thickness of 3 cm.

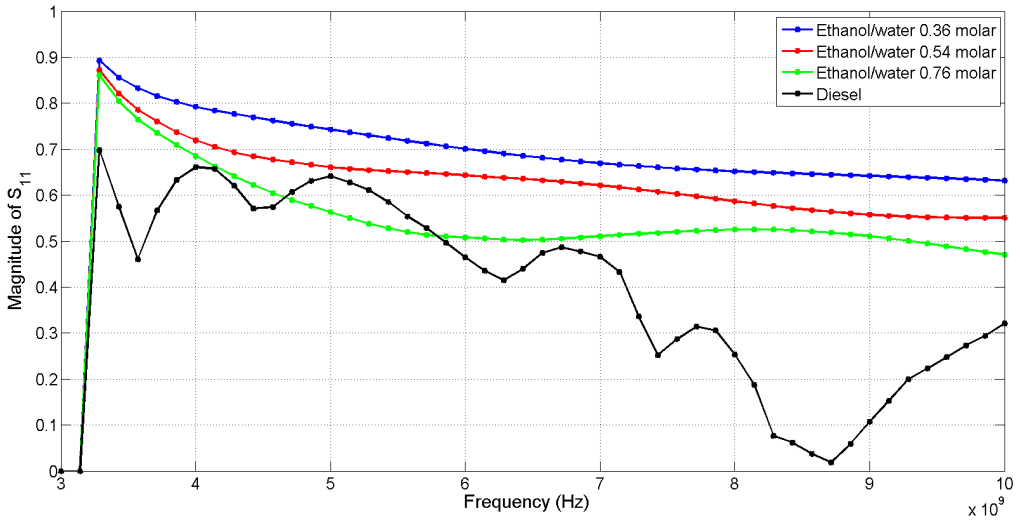

Figure 5.13: The magnitude of the simulated reflection coefficient for the three mixtures of ethanol/water and diesel with a thickness of 1 cm.

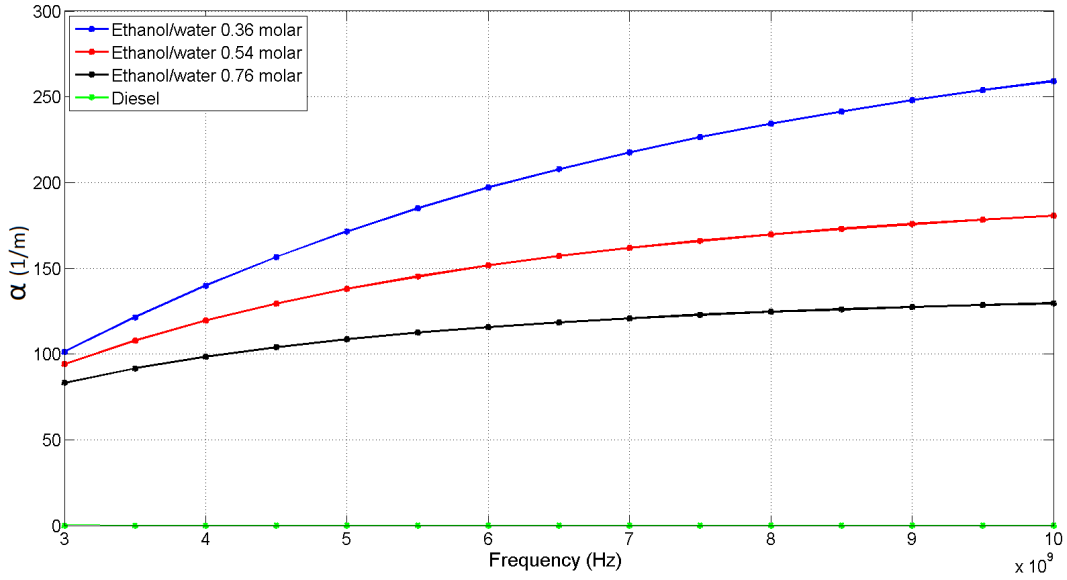

Figure 5.14: The α value for the three mixtures of ethanol/water and diesel.

The above mentioned behavior was not the case for diesel as a material with a low dielectric constant and a low loss factor. According to Figures 5.12 and 5.13, for diesel, some oscillations occurred in the magnitude of the simulated reflection coefficient over the whole frequency range, which were due to secondary reflections. It was therefore possible to extract the thickness information from the reflected signal. In addition, the α value was zero for diesel as it is shown in Figure 5.14. Accordingly, the microwave could radiate through the layer without attenuation.

The thickness estimation procedure was repeated for diesel but in a broader thickness range 0.5–5 cm. In case of each actual thickness, the total deviation between the transformed reflection coefficient and the corresponding elements of the thickness lookup matrix was calculated. Figures 5.15 and 5.16 show the total deviation versus each individual actual thickness value of diesel for the thickness ranges 0.5–3 cm and 3.5–5 cm, respectively. For example as shown in Figure 5.15, for actual thickness of 0.5 cm, it was found that the total deviation was minimum for the thickness value of 0.5 cm in the lookup matrix. Therefore, the estimated thickness was assumed to be 0.5 cm. In the case of actual thickness of 5 cm for instance, as shown in Figure 5.16, the minimum occurred for the thickness value of 4.2 cm in the lookup matrix, which represented the estimated thickness. Thus, it was concluded that unlike the mixtures of ethanol/water, the minimum total deviation was an absolute minimum for diesel layers with different actual thickness values, and results were robust.

Figure 5.17 shows the result of the thickness estimation for this fluid in the range 0.5–5 cm. The mean value of the estimation error was calculated to be 6.37% in this range, and therefore the estimated and actual thickness values were in a good agreement.

On the whole, it was concluded that the maximum detectable thickness depended on the relative permittivity of the MUT layer such that:

- According to Figure 3.9(a), for materials with lower dielectric constants, the magnitude of the reflection coefficient was lower, and therefore a larger fraction of microwaves were transformed rather than reflected. Accordingly, the waves were transmitted deeper through the MUT layer and the maximum detectable thickness increased.

- For a low-loss fluid such as diesel, the thickness estimation method gave satisfactory results for both thin (up to 1 or 2 cm) and thick layers (3–5 cm). However, in the case of MUTs with high or intermediate loss factors such as ethanol/water mixtures, the thickness estimation technique provided acceptable results only for layers up to 1 cm.

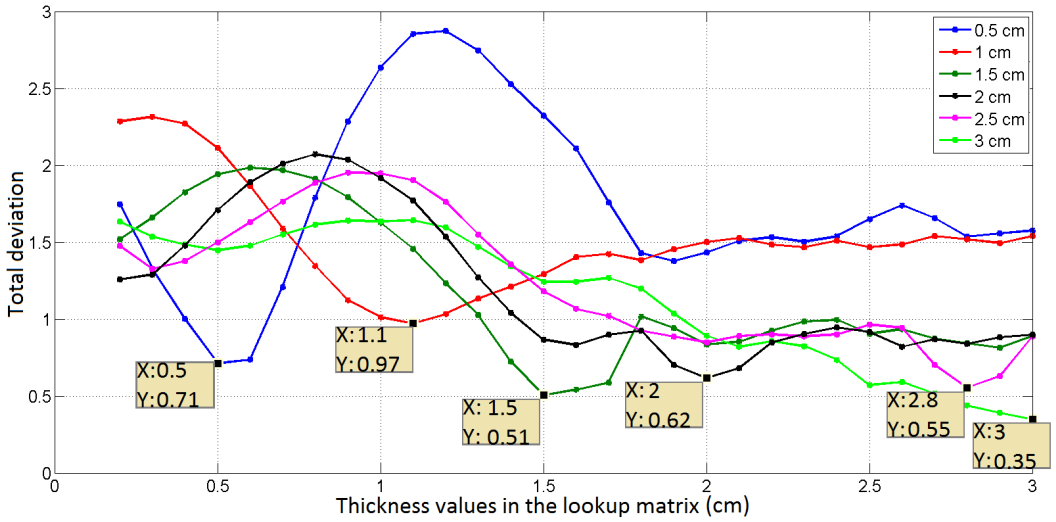

Figure 5.15: Total deviation between the transformed reflection coefficient and the corresponding elements of the thickness lookup matrix in estimating the thickness of diesel in the range 0.5–3 cm. The amount of minimum total deviation is highlighted for each actual thickness value.

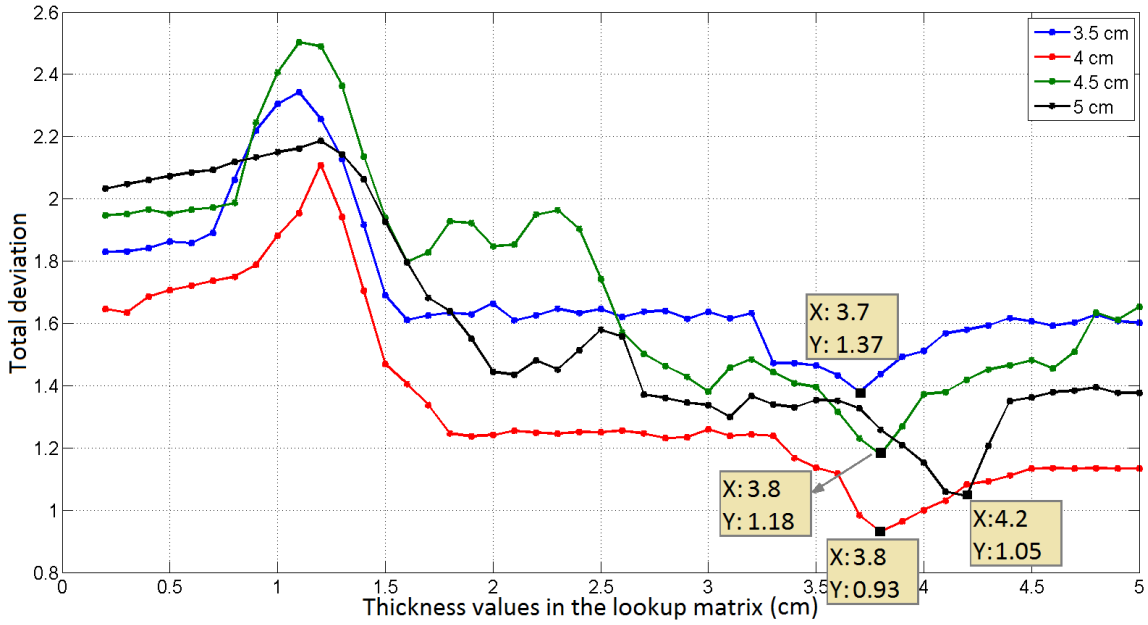

Figure 5.16: Total deviation between the transformed reflection coefficient and the corresponding elements of the thickness lookup matrix in estimating the thickness of diesel in the range 3–5 cm. The amount of minimum total deviation is highlighted for each actual thickness value.

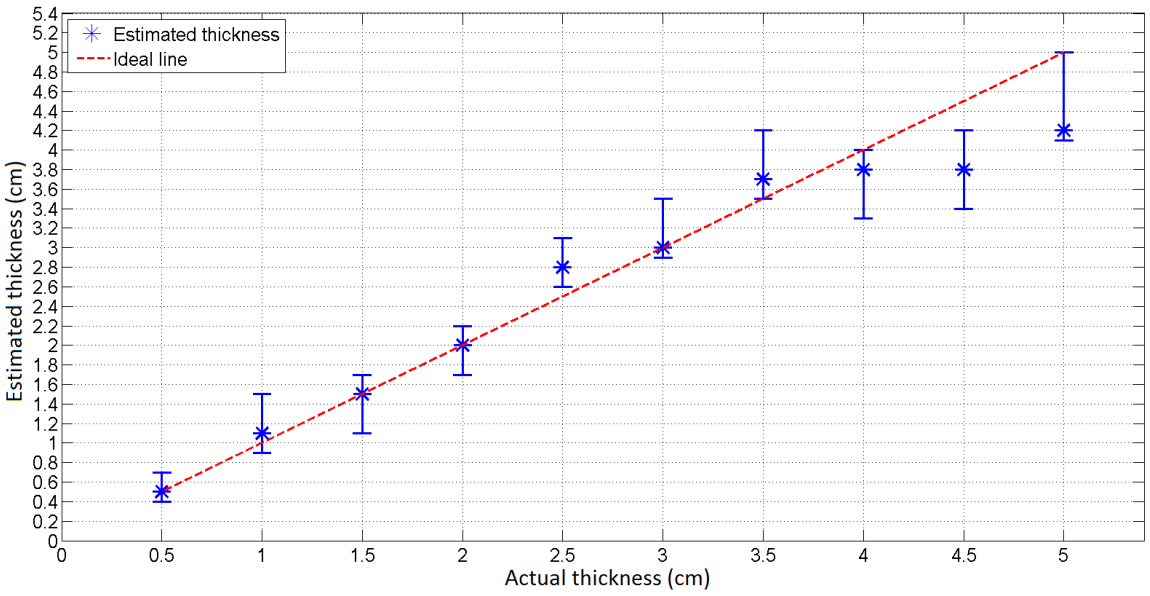

Figure 5.17: Result of the thickness estimation for diesel in the thickness range 0.5–5 cm

This page is intentionally left blank

Chapter 6

Conclusion

The feasibility of using an open-ended waveguide sensor and a reflection coefficient measurement technique for estimating the relative permittivity and thickness of dielectric layers in the thickness range 0.5–5 cm was investigated in this thesis.

Through an experimental procedure, the reflection coefficient for several fluids in the microwave frequency range (0.5–10 GHz) was measured. The measured data was calibrated by an equivalent simulation model and converted to the transformed reflection coefficient. Furthermore, by using this model, a permittivity lookup matrix and a thickness lookup matrix were generated. The former provides the simulated reflection coefficient as a function of permittivity ($1 \leq \varepsilon_r^{'} \leq 30$, $1 \leq \varepsilon_r^{''} \leq 17$) and frequency ($3\,GHz \leq f \leq 10\,GHz$). The latter gives the simulated reflection coefficient as a function of thickness ($0.2\,cm \leq d \leq 5\,cm$) and frequency ($3\,GHz \leq f \leq 10\,GHz$). The matrix element with the minimum deviation from the transformed reflection coefficient was corresponded to the estimated relative permittivity or thickness. In other words, the matrices created a link between the transformed reflection coefficient and the relative permittivity or thickness. This was the main contribution of the project.

The reflection coefficient of three ethanol/water mixtures with ethanol concentration of 0.36, 0.54, and 0.76 molar and thickness of 3 cm was measured in the frequency range 0.5–10 GHz using the experimental setup. The relative permittivity of the three mixtures was estimated in the frequency range 4–10 GHz using the permittivity lookup matrix and the transformed reflection coefficients. There was a good agreement between the estimated and actual relative permittivity in the range 4–6 GHz such that the mean value of the estimation error was found to be 20.21%, 11.37%, and 3.80% for ethanol/water 0.36, 0.54, and 0.76 molar, respectively. The lower permittivity fluid resulted in a better permittivity estimation.

For frequencies higher than 6 GHz, the result of the relative permittivity estimation was not acceptable. This could be due to interference between the dominant mode and higher order modes in the waveguide, which occurred at high frequencies. The simulation model was perfectly symmetrical, and therefore some of the higher order modes were not generated in the simulated waveguide. However, the experimental setup was not symmetrical, and some additional higher order modes could interfere with the dominant mode.

By measuring and calibrating the reflection coefficient of the above three mixtures in the thickness range 0.5–3 cm, the thickness was estimated using the thickness lookup matrix. There was a satisfactory agreement between the estimated and actual values for thinner layers (0.5–1 cm). The mean value of the estimation error for ethanol/water 0.36, 0.54, and 0.76 molar was 15.00%, 20.00%, and 13.25%, respectively. However, it was found that the measured reflection coefficient was almost independent of the thickness variations for thickness values higher than 1 cm. Therefore, the results of the thickness estimation were not acceptable for layers thicker than 1 cm.

It was found that in the case of diesel, as a material with a low loss factor, the effect of the thickness variations on the measured reflection coefficient was more significant, and changing the thickness changed the reflection coefficient curve clearly. Hence, the reflection coefficient for this fluid was measured in a broader thickness range 0.5–5 cm, and the thickness was estimated using the transformed reflection coefficients and the thickness lookup matrix. There was a good agreement between the estimated and actual thickness values for diesel in this range such that the mean value of the thickness estimation error was 6.37%. Therefore, it was concluded that the maximum detectable thickness depended on the loss factor of the fluid. In the case of low-loss fluids, the thickness estimation method gave satisfactory results for both thin (up to 1 or 2 cm) and thick layers (3–5 cm). On the contrary, for a fluid with a high or an intermediate loss factor, the thickness estimation technique gave good results only for layers thinner than 1 cm.

6.1 Further Work

In this section some suggestions for future works are provided.

- In order to estimate the relative permittivity of a material with a dielectric constant ($\varepsilon_r^{'}$) higher than 30 and a loss factor ($\varepsilon_r^{''}$) higher than 17, the generated permittivity lookup matrix should be expanded by performing extra simulations. Additionally, in order to improve the resolution, more simulations are required.

- In this study, the relative permittivity and thickness were estimated by assuming that one of them was known. Some extra work should be done to combine these two estimation procedures and estimate both, the relative permittivity and thickness of a fluid, simultaneously. A suggested solution is to generate a 3D matrix whose elements are simulated reflection coefficients as a function of frequency, relative permittivity, and thickness.

- It was concluded that the both proposed relative permittivity and thickness estimation methods provided acceptable results in the case of low-loss materials. Additionally, according to Eq. 2.12 and as shown in Figure 2.1, at frequencies less than 10 GHz, the loss decreases by reducing the frequency. Therefore, it is desirable to reduce the waveguide cutoff frequency in order to allow propagation of signals with lower frequencies. One possible solution is to fill the waveguide with a dielectric material. In this case, the new cutoff frequency is calculated from Eq. 2.33.

- The feasibility of the thickness estimation method for estimating the thickness of low-loss layers thicker than 5 cm should be evaluated.

- The amount of energy radiated through the MUT layer can be increased using two horn antennas (one as a transmitter and the other one as a receiver) instead of using a rectangular waveguide. By doing so, the microwaves will travel deeper through the layer and the maximum detectable thickness will be increased.

- The feasibility of using the presented approach in this thesis for estimating the thickness and permittivity of gas hydrates in pipelines should be investigated.

This page is intentionally left blank

References

[1] B. Tohidi, "Advances in avoiding gas hydrate problem," available from: https://www.spe-uk.org/aberdeen/wp-content/uploads/2014/01/SPE-Presentation-in-Edinburgh-March-2014-1.pdf at 12.11.2015.

[2] L. Ruffinea, J. Donvala, and J. Charloua, "Experimental study of gas hydrate formation and destabilisation using a novel high-pressure apparatus," *Marine and Petroleum Geology*, vol. 27, pp. 1157–1165, June 2010.

[3] H. Haghighi, R. Azarinejad, A. Chapoy, A. Anderson, and B. Tohidi, "Avoiding gas hydrate problems," *SPE Europec/EAGE Annual Conference and Exhibition*, 11-14 June 2007, London, UK.

[4] T. Jakobsen and K. Folgerø, "Dielectric measurements of gas hydrate formation in water-in-oil emulsions using open-ended coaxial probes," *Measurement Science and Technology*, vol. 8, pp. 1006–1015, April 1997.

[5] D. J. Griffiths, *Introduction to Electrodynamics*. Pearson, 2014, 4th edition.

[6] N. E. Hill, W. E. Vaughan, A. H. Price, and M. Davies, *Dielectric Properties and Molecular Behaviour*. Van Nostrand Reinhold, 1969, 1st edition.

[7] K. Folgerø, *Coaxial sensors for broadband complex permittivity measurements of petroleum fluids*. PhD thesis, Department of Physics, University of Bergen, 1996.

[8] K. Cole and R. Cole, "Dispersion and absorption in dielectrics," *The Journal of Chemical Physics*, vol. 9, pp. 341–352, February 1941.

[9] D. R. Lide, *CRC Handbook of Chemistry and Physics*. CRC Press, 2004, 48th edition.

[10] M. L. Solberg, *Near-surface petrochemical sensing using coplanar waveguides*. Master thesis, Department of Physics, University of Bergen, 2015.

[11] "The leader in millimeter-wave technology and solutions," available from: http://www.millitech.com/MMW-Antenna-LinearCircularPolarizer.htm at 27.03.2016.

[12] "Resources and analysis for electronics engineers," available from: http://www.radio-electronics.com/ at 22.12.2015.

[13] "All about circuits," available from: http://www.allaboutcircuits.com/ at 28.03.2016.

[14] G. H. Bryant, *Principles of Microwave Measurements*. Peregrinus on behalf of Institution of Electrical Engineers, 1993, 1st edition.

[15] L. F. Chen, C. K. Ong, C. P. Neo, V. V. Varadan, and V. K. Varadan, *Microwave Electronics: Measurement and Materials Characterization*. Wiley, 2004, 1st edition.

[16] A. V. Hippel, *Dielectric Materials and Applications*. Wiley, 1954, 1st edition.

[17] Z. Bayati, *Hydrate Monitoring using Capacitive Sensors.* Master thesis, Department of Physics, University of Bergen, 2013.

[18] Z. Haq, *Applied Measurement Systems.* In Tech, 2012, 1st edition.

[19] A. M. Nicholson and G. F. Ross, "Measurement of the intrinsic properties of materials by time domain techniques," *IEEE Transactions on Instrumentation and Measurement*, vol. 19, pp. 377–382, November 1970.

[20] W. B. Weir, "Automatic measurement of complex dielectric constant and permeability at microwave frequencies," *Proceedings of the IEEE*, vol. 62, pp. 33–36, January 1974.

[21] K. Folgerø, T. Friiso, J. Hill, and T. Tjomsland, "A broad-band and high-sensitivity dielectric spectroscopy measurement system for quality determination of low-permittivity fluids," *Measurement Science and Technology*, vol. 6, pp. 995–1008, February 1995.

[22] K. Folgerø, "Broad-band dielectric spectroscopy of low-permittivity fluids using one measurement cell," *IEEE Transaction on Instrumentation and Measurement*, vol. 47, pp. 881–885, August 1998.

[23] M. Karimi, *Permittivity measurements using dual open ended coaxial probes.* Master thesis, Department of Physics, University of Bergen, 2012.

[24] K. Haukalid, *Den coplanare bolgelederen som permittivitetssensor.* Master thesis, Department of Physics, University of Bergen, 2011.

[25] V. V. Varadan, R. D. Hollinger, D. K. Ghodgaonkar, and V. K. Varadan, "Free space, broadband measurements of high temperature, complex dielectric properties at microwave frequencies," *IEEE Transaction on Instrumentation and Measurement*, vol. 40, pp. 842–846, October 1991.

[26] K. T. Mathew and U. Raveendranath, "Waveguide cavity perturbation method for measuring complex permittivity of water," *Microwave and Optical Technology Letters*, vol. 6, pp. 104–106, February 1993.

[27] V. Subramanian, V. Sivasubramanian, V. R. K. Murthy, and J. Sobhanadri, "Measurement of complex dielectric permittivity of partially inserted samples in a cavity perturbation technique," *Microwave and Optical Technology Letters*, vol. 67, pp. 279–282, September 1996.

[28] S. Rao, *The Finite Element Method in Engineering.* Elsevier, 2010, 5th edition.

[29] P. Petong, R. Pottel, and U. Kaatze, "Water-ethanol mixtures at different compositions and temperatures," *The Journal of Physical Chemistry A*, vol. 104, pp. 7420–7428, July 2000.

[30] S. G. Johnson, "A brief introduction to the theory and practice of perfectly matched layer," available from: http://math.mit.edu/ stevenj/18.369/pml at 22.03.2016.

[31] K. Folgerø, "Bilinear calibration of coaxial transmission/reflection cells for permittivity measurement of low-loss liquids," *Measurement Science and Technology*, vol. 7, pp. 1260–1269, June 1996.

Appendix A

Coefficients of the Bilinear Transformation

The A, B, and C coefficients for three calibration fluids: water, air, and mixture of ethanol/water 0.76 molar ($x_e = 0.76$).

Table A.1: The A, B, and C coefficients in the bilinear transformation.

Frequency (GHz)	**A**	**B**	**C**
3*	-	-	-
3.5	-0.142 + 0.680i	0.643 + 0.175i	0.071 + 1.040i
4	0.619 + 1.090i	-0.442 – 0.668i	-1.283 + 0.076i
4.5	-0.508 + 3.119i	-1.258 + 0.775i	0.552 – 2.421i
5	1.451 – 0.412i	0.232 – 0.245i	-0.151+ 0.048i
5.5	0.450 + 1.054i	0.324 – 0.135i	0.114 + 0.818i
6	-4.064 – 3.539i	1.717 – 0.849i	-2.371 – 4.227i
6.5	-0.658 – 1.417i	0.030 – 0.915i	1.521 – 0.898i
7	-0.591 – 0.412i	-0.476 – 0.152i	1.245 + 0.424i
7.5	-0.422 – 0.459i	-0.392 + 0.246i	0.219 + 1.282i
8	-0.371 – 0.188i	0.075 + 0.356i	-0.899 + 0.841i
8.5	-0.596 – 0.140i	0.404 + 0.169i	-1.176 – 0.710i
9	-0.278 + 1.517i	0.712 – 0.398i	-1.213 + 1.635i
9.5	-0.182 + 0.610i	0.082 – 0.551i	-1.107 – 0.154i
10	-0.303 + 0.495i	-0.389 – 0.382i	-0.231 – 1.023i

* f=3 GHz is below the waveguide cutoff frequency so the amounts of A, B, and C are not relevant at this frequency.

This page is intentionally left blank

Appendix B

Content of the CD

The CD includes:

- The real part of the generated permittivity lookup matrix (Permittivity matrix/Real)
- The imaginary part of the generated permittivity lookup matrix (Permittivity matrix/Imaginary)
- The real part of the generated thickness lookup matrix for ethanol/water 0.36 molar (Thickness matrix/0.36 molar/Real)
- The imaginary part of the generated thickness lookup matrix for ethanol/water 0.36 molar (Thickness matrix/0.36 molar/Imaginary)
- The real part of the generated thickness lookup matrix for ethanol/water 0.54 molar (Thickness matrix/0.54 molar/Real)
- The imaginary part of the generated thickness lookup matrix for ethanol/water 0.54 molar (Thickness matrix/0.54 molar/Imaginary)
- The real part of the generated thickness lookup matrix for ethanol/water 0.76 molar (Thickness matrix/0.76 molar/Real)
- The imaginary part of the generated thickness lookup matrix for ethanol/water 0.76 molar (Thickness matrix/0.76 molar/Imaginary)
- The real part of the generated thickness lookup matrix for diesel (Thickness matrix/diesel/Real)

- The imaginary part of the generated thickness lookup matrix for diesel (Thickness matrix/diesel/Imaginary)